INVESTIGATION OF PHOTODETECTORS BASED ON III-NITRIDE AND METAL OXIDE THIN FILMS DEPOSITED BY ATOMIC LAYER DEPOSITION

A THESIS SUBMITTED TO
THE GRADUATE SCHOOL OF ENGINEERING AND SCIENCE
OF BILKENT UNIVERSITY
IN PARTIAL FULFILLMENT OF THE REQUIREMENTS FOR
THE DEGREE OF
MASTER OF SCIENCE
IN
ELECTRICAL AND ELECTRONICS ENGINEERING

By
Burak Tekcan
May, 2015

INVESTIGATION OF PHOTODETECTORS BASED ON III-NITRIDE AND METAL OXIDE THIN FILMS DEPOSITED BY ATOMIC LAYER DEPOSITION
By Burak Tekcan
May, 2015

We certify that we have read this thesis and that in our opinion it is fully adequate, in scope and in quality, as a thesis for the degree of Master of Science.

Asst. Prof. Dr. Ali Kemal Okyay(Advisor)

Prof. Dr. Oğuz Gülseren

Assoc. Prof. Dr. Hüsnü Emrah Ünalan

Approved for the Graduate School of Engineering and Science:

Prof. Dr. Levent Onural
Director of the Graduate School

ABSTRACT

INVESTIGATION OF PHOTODETECTORS BASED ON III-NITRIDE AND METAL OXIDE THIN FILMS DEPOSITED BY ATOMIC LAYER DEPOSITION

Burak Tekcan
M.S. in Electrical and Electronics Engineering
Advisor: Asst. Prof. Dr. Ali Kemal Okyay
May, 2015

Gallium Nitride (GaN), one of the most attractive optoelectronic materials today with a direct wide band gap of 3.4eV and high electron saturation velocity of, has found many applications from blue/UV LEDs to UV photodetectors, from high electron mobility transistors (HEMT) to solar cells. Traditional techniques to grow GaN films require high temperature (over 600°C) processes. Such techniques cannot be used to synthesize GaN films on temperature sensitive substrates such as plastics or even paper for large area optoelectronic applications. To circumvent this setback, atomic layer deposition (ALD) stands out with its unique features such as low temperature process, precise thickness control and step coverage.

Our work marks the demonstration of the first optical device on hollow cathode plasma assisted atomic layer deposition (HCPA-ALD) grown GaN films. The fabricated devices showed promising electrical and optical performance. A UV/VIS contrast ratio of 15 is obtained with very low dark current of 14pA at 20V applied bias. Annealing the films improved the device performance. Dark current was reduced more than two orders of magnitude while the responsivity was increased by two times.

In the second part of the thesis, optoelectronic device applications on ALD grown ZnO layers will be presented. ZnO is also an attractive wide direct band gap semiconductor. It is utilized in many optical devices such as photodetectors and solar cells as well as thin film transistors and biomedical applications. In this work, device applications of ZnO on Silicon heterojunctions are investigated. A high rectification ratio of 10^3 is achieved with 80°C grown ZnO-Si heterojunction photodiodes. High responsivity values are also recorded for these devices. At 350nm incident wavelength maximum responsivity of 35mA/W and at 585nm incident wavelength maximum responsivity of 90mA/W are obtained.

Keywords: Gallium Nitride (GaN), Zinc Oxide (ZnO), atomic layer deposition, metal-semiconductor-metal, p-n heterojunction photodiode.

ÖZET

ATOMİK KATMAN KAPLAMA TEKNİĞİ İLE III-NİTRÜR VE METAL-OKSİT BİLEŞİK TEMELLİ FOTODEDEKTÖRLERİN ARAŞTIRILMASI TÜRKÇE BAŞLIK

Burak Tekcan
Elektrik ve Elektronik Mühendisliği, Yüksek Lisans
Tez Danışmanı: Asst. Prof. Dr. Ali Kemal Okyay
Mayıs, 2015

3.4 eVlik geniş bant aralığına ve yüksek elektron doyum hızına sahip olan Galyum Nitrür (GaN) günümüzde en gözde optoelektronik malzemelerden biridir ve kendine mavi/UV LEDlerden UV fotodetektörlere, yüksek elektron mobiliteli tranzistörlerden güneş gözelerine kadar birçok uygulama alanı bulmuştur. GaN film üretimi için kullanılan geleneksel yöntemler yüksek sıcaklıkta (600°C'den büyük) işlemler gerektirmektedir. Bu tür yöntemler ile plastik ve hatta geniş alanlı optoelektronik uygulamalarda kullanılan kâğıt gibi ısıya karşı duyarlı alttaşlar üzerinde GaN sentezlenememektedir. Bu dezavantajın önüne geçebilmek için düşük sıcaklıkta işlem yapabilme, hassas kalınlık kontrolü ve adım kapsaması gibi kendine has özellikleri sayesinde atomik katman kaplama (ALD) öne çıkmaktadır.

Çalışmamızda dünyada ilk defa oyuk katot plazma destekli atomik katman kaplama (HCPA-ALD) ile büyütülmüş GaN temelli optik cihazlar gösterilmiştir. Üretilen cihazlar umut verici elektriksel ve optik performans göstermiştir. 20V voltaj uygulandığında 14pA'lik oldukça düşük karanlık akım gözlemlenmiş, ultraviyole/görünür ışık kontrast oranı 15 olarak ölçülmüştür. Filmlerin tavlaması cihaz performansında artışa neden olmuştur. Karanlık akım 100'de birine düşerken duyarlılık 2 katına çıkmıştır.

Tezin ikinci kısmında ise ALD ile büyütülmüş ZnO katmanları üzerinde optoelektronik cihaz uygulamaları sunulmaktadır. ZnO geniş ve doğrudan bant aralığına sahip literatürde çok çalışılmış bir yarıiletkendir. Hâlihazırda fotodetektörler, güneş gözeleri ve ince-film tranzistörler gibi birçok optik cihazda ve biyomedikal uygulamalarda kullanılmaktadır. Bu çalışmada Silisyum üzerinde

ZnO heteroeklem cihaz uygulamaları araştırılmıştır. 80°C'de büyütülmüş ZnO-Si heteroeklem fotodiyotlarda 10^3 gibi yüksek bir doğrultma elde edilmiştir. Bu cihazlarda ayrıca yüksek duyarlılık değerleri de elde edilmiştir. 350nm dalgaboyunda ışık uygulandığında 35mA/W duyarlılık ve 585nm dalgaboyunda ise 90mA/W duyarlılık gözlemlenmiştir.

Anahtar sözcükler: ZnO, GaN, atomik katman kaplama, metal-yariletken-metal, p-n heteroeklem fotodiyot.

Acknowledgement

First of all, I would like to express my sincere gratitude to Dr. Ali Kemal Okyay for his guidance, knowledge and motivation throughout my studies. I would like to offer my deepest appreciation to him providing me high quality education for my future carrier. In addition, I would like to convey my deepest regards to Dr. Necmi Bıyıklı and Dr. Ammar Nayfeh for sharing their valuable knowledge and continuous supports. Moreover, I would like to thank Prof. Oğuz Gülseren and Dr. Hüsnü Emrah Ünalan for improving quality of my work and my thesis with their helpful comments and suggestions.

The work reported in the thesis is supported by (Scientific and Technological Council of Turkey) TUBITAK, with grant numbers 109E044, 112E052, 112M004, 112M482 and 113M815. I would like to thank TUBITAK BIDEB 2210-C M.Sc. Fellowship.

Special thanks belong to my friends, Barış Saydere, Alican Noyan, İnci Dönmez, Levent Erdal Aygün, Sami Bolat, Dr. Fatih Bilge Atar, Feyza Bozkurt Oruç, Deniz Kocaay, Pelin Kübra İşgör, Berk Berkan Turgut, Volkan Hünerli and my mentor Dr. Sabri Alkış for wonderful memories we spent together.

I thank Okyay group family members, Ayşe Özcan, Furkan Çimen, Enes Battal, Elif Özgöztaşi, Muhammad Maiz Ghauri, Yunus Emre Kesim, Dr. Manoj Kumar, Amin Nazirzadeh, Şeyma Canik and Ali Cahit Köşger for being nice friends to me and UNAM cleanroom team Semih Yaşar, Fikret Piri and Adem Saraç for their cooperation.

I thank all my collaborators Dr. Çagla Özgit-Akgün, Dr. Eda Goldenberg, Dr. Manoj Kumar, Dr. Mehmet Solmaz, Ali Haider, Seda Kizir for their help and contribution to our work. For those whom I have not mentioned above, I sincerely thank all people I met during last three years in UNAM.

I am really grateful to my parents Rukiye and Cemalettin Tekcan and my dear brother Göktuğ Tekcan, who always support me to pursue my dreams. I would be very happy if I managed to be a good son.

Last but not the least, I would like to specially thank my lovely girlfriend Merve Marçalı, who was always with me during happy and sad moments with her endless support and warmest love. No word would be good enough to express my appreciation to her.

Contents

List of Figures

List of Tables

Chapter 1

Introduction

1.1 Gallium Nitride Based Optoelectronic Devices

GaN is an attractive semiconductor due to its unique optical and electronic properties. It has direct band gap of 3.4eV and high electron saturation velocity of 3×10^7cm/s that are useful for many optoelectronic devices. Moreover, its chemical stability and endurance in extreme conditions puts GaN at the forefront of high performance electronic and optoelectronic applications. Today, UV photodetectors, blue/UV LEDs, violet lasers, high speed FETs, HEMT devices, and high power RF transistors are mainly dependent on GaN technology.

1.1.1 GaN based photodetectors

Today, GaN based UV photodetectors are being used in various applications. In astronomy, for instance, locations of newborn galaxies, which radiate UV light, can be detected using UV photodetectors. In addition, satellites ensuring telecommunication lines uses UV signals to transfer data between each others, UV photodetectors are used at the receiver ends of the communication lines. Moreover, engine control and missile and flame detection techniques use UV photodetectors. In these areas, GaN technology is dominant over Silicon and other semiconductors.

GaN was a rock star in 1990s after its successful growth on sapphire substrate, which later brought a Nobel Physics Prize in 2014 to the invention of blue LEDs. After the invention, many reports were published on GaN based photodetectors. Very low dark currents with high quantum efficiencies were reported [4]. Due to the internal gain mechanism quantum efficiencies more than 100% were achieved in GaN based photodetectors [5]. However, gain is a limiting factor in temporal response. To overcome this problem, smaller device features with metal-semiconductor-metal structures were used and picosecond response times are achieved [6]. One of the major problems of GaN based photodetectors is that trap levels exist at the interface due to semiconductor imperfections. To eliminate these effects, various capping layers and different contact materials were used [7, 8]. To further improve the UV responsivity of devices, plasmonics and nanostructures were used [9, 10, 11]. In addition, relatively low efficiency devices were reported based on GaN on Silicon [12]. However, the techniques reported above rely on high temperature processes, which make temperature sensitive processes impossible.

1.1.2 Motivation

Achieving GaN devices at low temperatures is a difficult task. Most commonly used methods for the deposition of GaN layers which are used for high-performance UV photodetectors, are metal organic chemical vapor deposition (MOVCD) [4, 7, 8, 12], molecular beam epitaxy (MBE) [13, 14, 15], and hydride vapor phase epitaxy (HVPE) [5, 6], nonetheless, integration of GaN devices with silicon CMOS VLSI and flexible electronics technology is hampered by high temperature requirements of these traditional growth techniques. At low temperatures there are other techniques to grow decent quality films such as sputtering [16] and pulsed laser deposition [17]. Among various deposition techniques, atomic layer deposition (ALD) technique holds great potential owing to its low temperature deposition and self-limiting growth in cyclic manner. ALD enables unique properties such as high uniformity over large area deposition, atomically sensitive thickness control and high conformality. Recently, it has been shown that low temperature growth of polycrystalline GaN is possible using hollow cathode plasma-assisted ALD (HCPA-ALD) technique [18]. However, suitability of HCPA-ALD grown GaN to optoelectronic device applications such as photodetectors need further investigation.

In this work, a proof-of-concept HCPA-ALD grown GaN based ultraviolet (UV) photodetectors are demonstrated. For this purpose, metal-semiconductor-metal (MSM) type photodetectors are designed and fabricated using CMOS-compatible standard micro-fabrication processes. To the best of our knowledge, this study represents the first demonstration of MSM UV photodetectors based on HCPA-ALD grown GaN.

1.2 ZnO Based Optoelectronic Devices

1.2.1 ZnO based photodetectors

Thin film semiconductor industry is an emerging area where many modern electronic and photonic devices are based on. Among others, ZnO is one of the most attractive semiconductors according to recent studies. Being a non-toxic semiconductor that can be deposited at low temperatures without sacrificing film quality, ZnO can be used as an alternative to Silicon in electrical and optoelectronic applications [19, 20]. Being transparent in the visible regime and electrically conducting, it is attractive for photovoltaic applications [20]. ZnO has a direct bandgap of 3.3eV enabling high absorption of high-energy photons. This is an attractive feature for solar cell and photodetector applications [21, 22, 23, 24, 25]. Up to date, many thin film based photodetectors in ultraviolet (UV) and visible (VIS) range are presented [26, 27, 28].

1.2.2 Motivation

ZnO can be deposited on diverse substrates using low pressure chemical vapor deposition (LPCVD) [20], RF magnetron sputtering [22, 23, 24, 29], DC magnetron sputtering [30], metal organic chemical vapor deposition (MOCVD) [31, 32] and spray pyrolysis method [33]. There are reports on p-i-n photovoltaic cells based on LPCVD grown ZnO [20]. Moreover, RF magnetron sputtering based n-ZnO/p-Si photodiodes are present in the literature [19, 22, 23, 29]. For example, RF magnetron sputtering based devices have a photocurrent of 11 mA/cm^2 at 5V reverse bias [19].

Besides other growth technologies, ZnO growth is possible using ALD [34, 35, 36, 37, 38, 39, 40]. Sequential pulsing of diethylzinc (DEZ$_n$) and water vapor (H_2O) into the chamber in a cyclic manner can achieve high quality ZnO thin films [41, 42]. However, ALD grown ZnO films are never been studied as active layer for optoelectronic applications. Unintentionally doped n-type ZnO layer is believed to be good fit for a p-n junction photodiode with its optical and electronic features especially in the UV range.

1.3 Thesis Overview

This thesis investigates possibility of III-Nitride (GaN) and Metal Oxide (ZnO) based photodetectors based on ALD growth.

Chapter 2 describes the atomic layer deposition technique, its features and applications. In the latter part, a brief basic semiconductor physics is introduced and mechanism of photodetection is explained.

Chapter 3 mentions the methods and techniques used for experimental procedures. The growth, device fabrication and characterization techniques are explained.

Chapter 4 discusses the results of the characterization of HCPA-ALD GaN based MSM photodetectors. Film quality and device performance are investigated in detail.

Chapter 5 shows the results and discussions on ZnO-Si heterojunction photodiodes based on ALD grown ZnO layer grown at different ambient temperatures. Electrical and optical characterizations are presented.

Chapter 6 summarizes the thesis pointing out the significant outcome of the study. This section also makes a projection on ALD based optoelectronic devices for future studies.

Chapter 2

Theoretical Background

2.1 Atomic Layer Deposition of III-Nitride and Metal-Oxide films

2.1.1 Introduction

Atomic layer deposition (ALD) is a special kind of chemical vapor deposition (CVD) technique, which is used for variety of applications in semiconductor industry. Desired chemicals are introduced into a reaction chamber in a cyclic manner. In every cycle, one atom thick layer of desired chemical is coated onto the surface. This technique is useful in terms of conformality and thickness controllability. ALD is a novel and easy-to-build tool in that sense, which opened up a way to grow high k dielectric materials for MOSFET gate oxides, capacitors and interconnects in Silicon chip technology. As the devices continue to shrink in size and functionality become more prominent with developing technology, high quality thin films deposition constitutes a special place. Achieving a conformal coverage of structures below 20nm with a desired crystal quality is definitely a big challenge.

Atomic layer deposition technique is first pronounced in late 1970s with a name "atomic layer epitaxy" as a thin film deposition technology [43]. This technique is developed to produce thin film electroluminescent displays flat panel displays with high k dielectric and large area devices [44]. For epitaxial growth, MOCVD and MBE has superior advantages compared to ALD, however, ALD began very popular after 1990s in the search for thin film Silicon microelectronics to achieve conformal films especially high k dielectrics [44]. However, optoelectronic devices based on active layers deposited by ALD is an unknown concept.

Recently, it has been shown that ALD technique can also be used for growing active layers of optoelectronic devices. Besides Silicon technology, there is a number of semiconducting materials such as III-Nitrides and Metal Oxides. Among these materials, GaN and ZnO are most attractive semiconductors. ALD growth of GaN and ZnO is possible using ALD technique. This study investigates the feasibility of those devices.

2.1.2 ALD Principle and Deposition Mechanism

Unlike any other chemical vapor deposition techniques ALD works in a cyclic routine and it is based on self-limiting surface reactions at the end of each cycle. One ALD cycle consists four steps which are 1) exposure of the first precursor (active material connect to a ligand group) 2) purging of the chamber 3) exposure of the second precursor 4) purging of the chamber again [1]. This process continues until the desired thickness is achieved. Since it is based on self-limiting process and progresses in cyclic manner, the thickness can be calculated simply by counting the total number of cycles and multiplying with the resulting thickness of a single cycle deposition.

A common example to illustrate ALD deposition is Aluminum Oxide (Al_2O_3) growth. Tri-methyl aluminum (TMA), which consists of one Aluminum atom (Al) connected to three methyl (CH_3) molecules, is used in general.

Upon exposure of the first precursor, TMA and hydroxyl group (at the surface) react each other, a methane (CH_4) molecule is released and Al atom is attached to the surface (See Figure 2.1a). Every Al atom finds an empty spot on the surface, until no empty spot remains. Excessive precursors are purged out as the second step (Figure 2.1b). Then, second precursor is introduced in which water molecules are used as Oxygen (O) source; O atoms connect to the Al atoms (Figure 2.1c). This is followed by purging of remaining water molecules and resulting CH_4 molecules (Figure 2.1d). The continuous purging is maintained with Nitrogen flow. This completes one cycle of an ALD process. Repetition of this cycle grows thicker films.

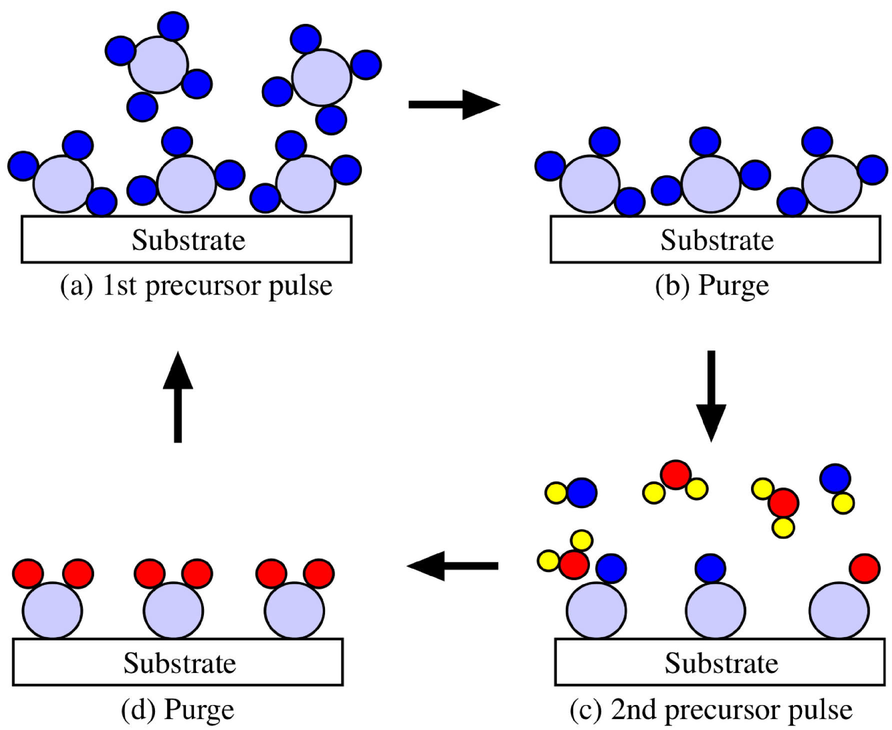

Figure 2.1: Illustration of basics atomic layer deposition technique

At this point, self-limiting behavior of ALD should be stressed. The saturation is reached if the pulse time of the precursor is long enough, also the precursor should not be decomposed during the reaction, as this will become a CVD type growth rather than ALD [1]. In ideal case, we assume that each cycle grows one monolayer, however, this is generally less than one monolayer [1]. Due to steric hindrances and limited number of reactive sites the growth rate decreases from the ideal case [1]. This is shown the in Figure 2.2a.

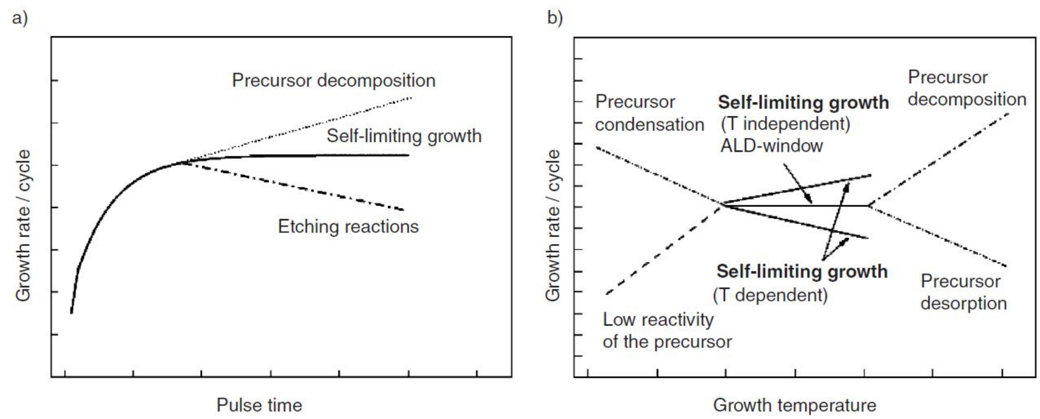

Figure 2.2: ALD growth rate with respect to pulse time. The self-limiting behavior is affected by the pulse time [1].

The self-limiting behavior of ALD is valid under certain conditions. ALD window describes the range of parameters for ideal conditions of deposition. There are many factors affecting the ideality and these factors are illustrated in the Figure 2.2b. For lower temperatures the factors such as condensation and incomplete reaction can occur which is due to insufficient thermal energy to break the precursor bonds and attach to the surface [2]. For higher temperatures, on the other hand, the chemicals could decompose or desorb so that the reaction cannot happen. These factors affect ALD operation and there is ALD operation is hindered out of the window [2].

2.1.3 Advantages and Disadvantages of ALD Technique

Compared to other techniques ALD has advantages and disadvantages that are listed below:

- ALD is a slow technique but deposits very conformal (Figure 2.3) and stoichiometric films.
- Superior thickness control is achieved, ultra thin films can be grown up to single monolayer, on the order of Angstroms.

- System is cheap and much simpler compared to MOCVD and MBE.
- Using liquid precursors for deposition
- Reaction temperature can be quite low.

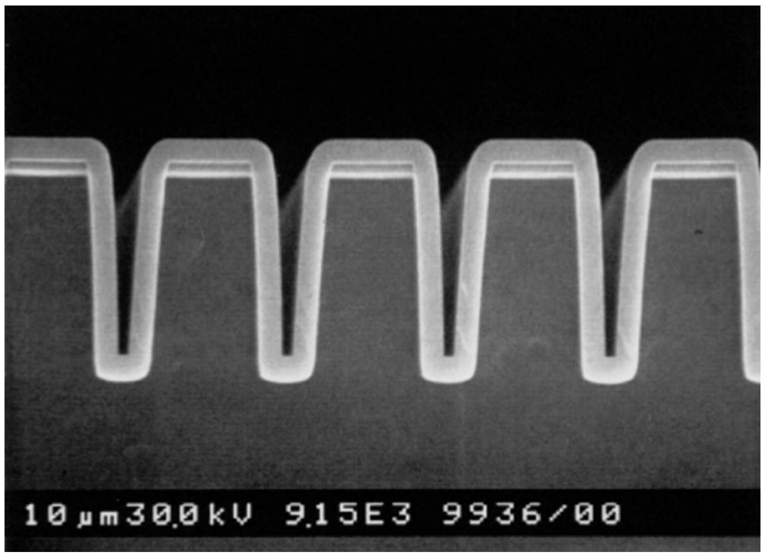

Figure 2.3: Cross-sectional SEM image of an ALD growth over the high-aspect ratio surface with great conformality[2].

2.1.4 Plasma Assisted ALD

In general ALD processes, thermal energy is used to supply the necessary energy for the reactions. However, for some processes, the required thermal energy desorbs or discomposes the precursors due to high temperature in the ambient. To circumvent this problem, required energy in injected by plasma generation. For instance, plasma assisted ALD (PA-ALD) is used to increase reactivity of NH_3 or N_2:H_2 gasses in order to deposit Nitride based semiconducting films such as GaN [18]. The plasma source does not eliminate the use of thermal energy, so that most of the PA-ALD systems include temperature and plasma source control to obtain high quality films.

2.1.5 ALD Reactors

ALD operation is done in reaction chambers. The precursors are connected to the valves which control the precursor volume as illustrated in Figure 2.4. During operation the dose volume is first filled by opening only the fill valve, and then emptied by opening only the empty valve [1]. The precursor is introduced into the chamber with carrier gas.

In most ALD systems, a carrier gas preferably Nitrogen gas flows continuously so that precursors are introduced and evacuated. The most advantages part of carrier gas is that the ALD cycle durations are shorter than no carrier gas systems [1]. The carrier gas should be inert because the gas should not react with the surface to create impurities [1].

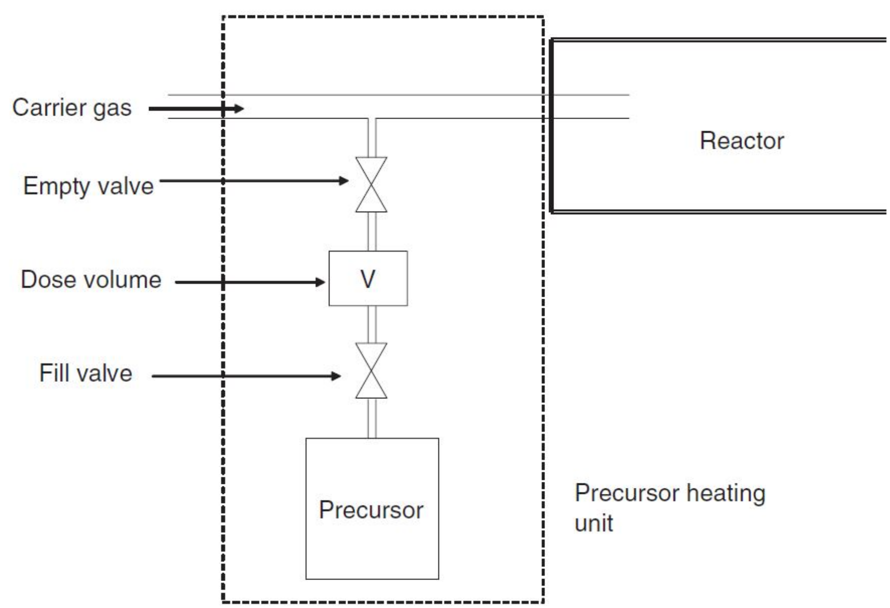

Figure 2.4: Schematic of a source setup with a precursor vessel, two on-off valves and a precursor dose controlling volume enclosed in a heating system, e.g. oven, maintaining the components at a common temperature [1].

There are three kinds of chamber geometries. These have name Cross-Flow Reactors, Perpendicular Flow Reactors and Radial-Flow Reactors (Figure 2.5). Ideally three systems should be same in terms of coating but there are small differences between these three.

For instance, cross-flow reactor has higher speed compared to perpendicular-flow reactor but its disadvantage comes from non-uniform films due to decomposition of the precursors [1].

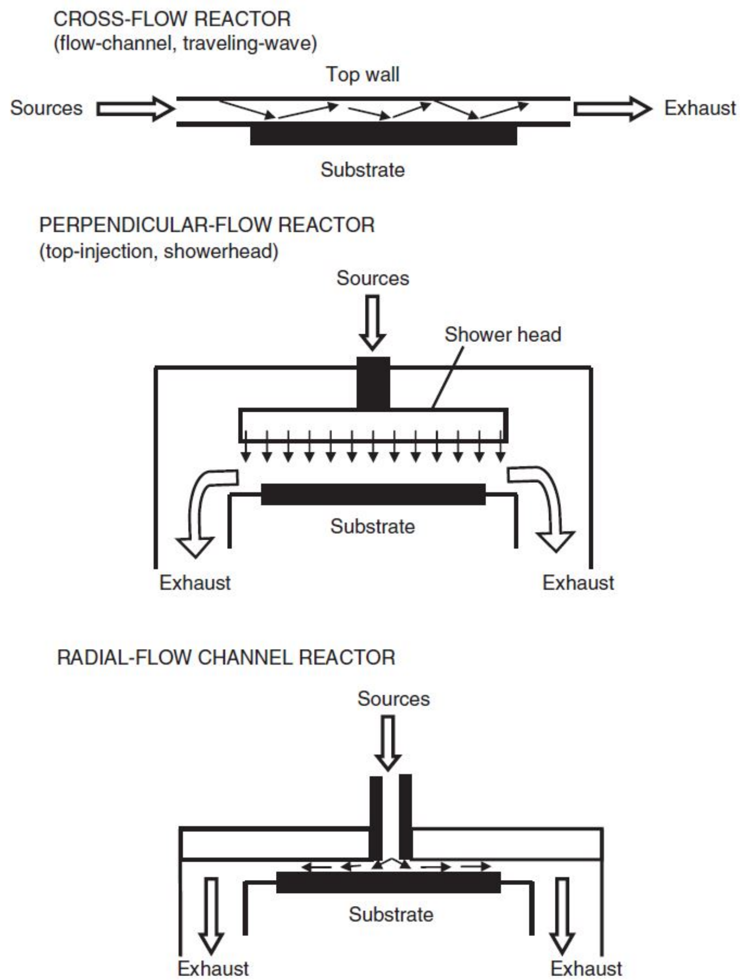

Figure 2.5: Three kinds of chamber reactor geometries [1].

2.1.6 Applications of ALD

There is a wide variety of usage of atomic layer deposition in todays world. Although it is slow process, conformality and high quality film growing makes ALD a useful technique. ALD is preferred in Thin Film Electroluminescent Displays (TFELs), Magnetic heads used in hard disks, microelectronics especially for high k dielectrics for MOSFETS and DRAMs, protective coatings for jewelry, thin film solar cells, optical aperture coatings, heterogeneous catalysts, powder and polymer coatings, coating for MEMS devices and many subareas in nanotechnology such as nanowire and nano-particle coatings etc. [1]. Lately, usage of ALD is also investigated for thin film transistors and optoelectronic devices, decent electrical performances are achieved. However, the quality of the resulting films are still under investigation.

2.1.7 Conclusion

Atomic layer deposition is a special kind of chemical vapor deposition, but it has very important features like self-limiting process and conformality, which make ALD a unique technique. The technique works in cycles so that the thickness is controlled easily. While the transistor sizes continue to shrink, high k dielectrics instead of SiO_2 are used and ALD is a very proper technique to grow such films on big area samples. These all make ALD is a promising technique for future semiconductor technologies.

2.2 Semiconductor Photodetector Basics

2.2.1 Basic Semiconductor Physics

In semiconductors, there is an energy gap between the highest energy level that is full of electrons and lowest energy level that is completely empty of electrons. Between these levels there are no available states. This energy gap is called band gap and it is one of the most important properties of semiconductors. The highest energy level with electrons is called valence band, whereas the lowest energy level that is empty is named conduction band. Electrons in conduction band are free to move in the semiconductor.

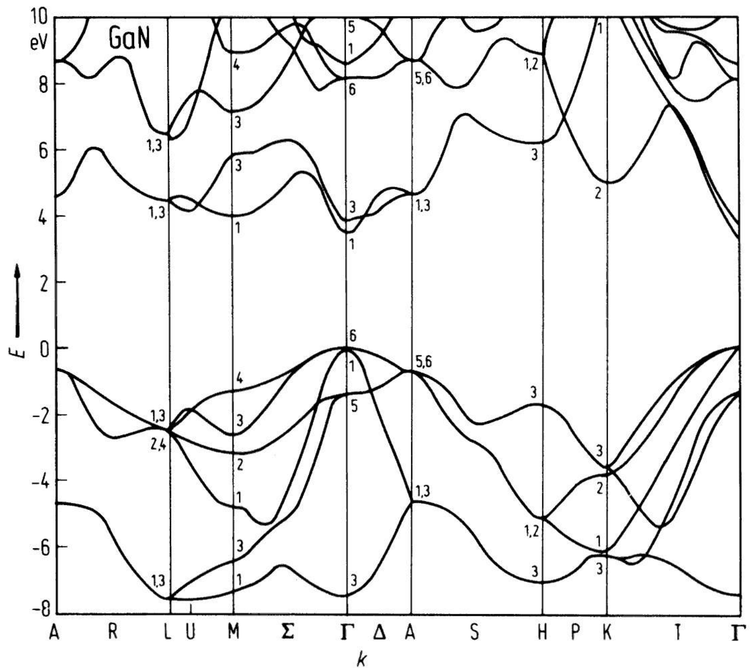

Figure 2.6: Electronic Band Diagram of Wurtzite GaN, calculated empirically [3].

The electronic band structure (E-k diagram) is determined by solving the Schrödinger's equation in a crystal semiconductor, the potential is periodic over the lattice (Bloch theorem), so that the solution of Schrödinger's equation can be found as

$$\Big[-\frac{\hbar}{2m}\nabla^2 + V(r)\Big]\phi(r,k) = E_k\phi_k(r,k) \tag{2.1}$$

$$\phi_k(r,k) = e^{jk.r}U_n(r,k) \tag{2.2}$$

ZnO and GaN are both direct-bandgap materials where the conduction band minimum and valence band maximum are at the same momentum. Having direct bandgap structure, semiconductors exhibit strong optical absorption near the bandgap energy. These materials are commonly used for optoelectronic applications because of their optical properties.

2.2.2 Optical Properties of Semiconductors

Photons and electrons interact with each other in a couple of ways. The mechanism of interband transition is of interest and it determines the photodetection mechanism. Given a sufficient energy that corresponds to the band gap energy of the semiconductor, electrons move from valence band to the conduction band. This transition creates a hole, absence of an electron; photon energy is converted into electrical energy. This is called optical absorption. The optical absorption forms the basis of todays photodetectors and LEDs.

The absorption coefficient is a measurable quantity; it defines the rate of absorption inside the crystal. The absorption coefficient can be calculated by the

$$\alpha(\lambda) = \frac{4\pi k(\lambda)}{\lambda} \tag{2.3}$$

where k(λ) can be determined by ellipsometry [45]. The absorption spectrum, assuming parabolic density of states, will follow $(\sqrt{h\nu - E_g})^{\gamma}$ with respect to energy.

Absorption coefficient can be determined by the reflection and transmission of the material. Reflection and transmission at normal incidence can be found as

$$R = \frac{(1 - n_r^2) + k_e^2}{(1 + n_r^2) + k_e^2} \tag{2.4}$$

and

$$T = \frac{(1 - R^2)e^{-\frac{4\pi x}{\lambda}}}{1 - R^2 e^{-\frac{8\pi x}{\lambda}}} \tag{2.5}$$

where n and k are the real and imaginary parts of refractive index, x and λ is the thickness of the films and wavelength of incident light respectively [46].

2.2.3 PN Junctions

P-N junctions are the most basic devices of semiconductor industry. The ability of rectification is used in MOSFETs, BJTs and diodes. In optoelectronics, however, they are utilized to collect electrons and holes that are generated by absorption. This process converts optical signal into electrical signal.

Conjugating p-type and n-type materials creates p-n junctions. Upon forming a junction, a depletion region forms at the interface in which mobile carriers are diffused opposite sides, while remaining ions create an electric field opposing the diffusion. At thermal equilibrium, there is no mobile carrier residing in the depletion region due to the electric field. The depletion region is important

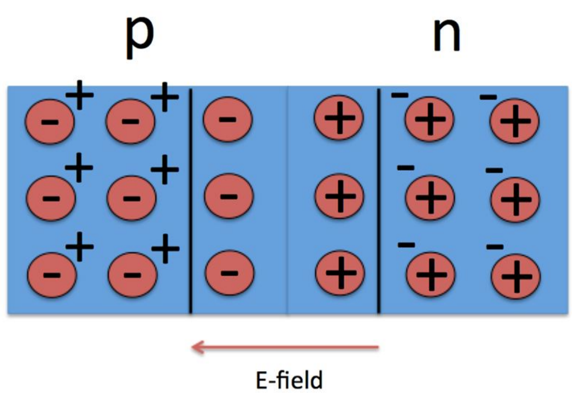

Figure 2.7: Schematic illustration of a homojunction pn diode, depletion region and internal built-in electric field.

in converting optical signal into electrical signal. Photogenerated electron hole pairs can only be converted into electrical signal if they are absorbed inside the depletion region. Those photogenerated electron hole pairs who reside outside the depletion region does not contribute to electrical current, they simply recombine after a short length. The width of the depletion region is given as

$$\omega_d = \sqrt{\frac{2(V_{bi} + V_{reverse})\epsilon_r \epsilon_0 (N_A + N_D)}{e(N_A N_D)}} \tag{2.6}$$

Electron hole pairs generated in the depletion layer, are swept away due to internal built-in E-field, therefore, such carriers can be collected by the contacts. Increasing the reverse bias voltage increases the depletion width so the total absorption to collection rate increases. The current density in p-n junction is

$$J = J_s \Big[e^{\frac{eV}{k_B T}} - 1 \Big] \tag{2.7}$$

where

$$J_s = \frac{eD_h}{L_h} p_{n_0} + \frac{eD_e}{L_e} n_{p_0} \tag{2.8}$$

which is the saturation current of pn junction under reverse bias [46].

2.2.4 Schottky Junctions

Schottky junction consists of a metal semiconductor junction. The work function of metal and Fermi level inside the semiconductor defines the band alignment at thermal equilibrium.

The difference of work function of metal, ϕ, and electron affinity, χ, of semiconductor creates a built-in potential so that a depletion region forms. The barrier height can be expressed as

$$q\phi_B = q(\phi_M - \chi) \tag{2.9}$$

Under depletion approximation the width W is

$$W = \sqrt{\frac{2\epsilon}{qN_D}\left(\phi_B - V_{bias} - \frac{kT}{q}\right)} \tag{2.10}$$

Thermionic emission is the main mechanism of Schottky junctions, under low bias. Majority carriers are dominant in Schottky junctions unlike pn junctions where minority carriers are important. This theory suggests that the carriers cannot pass the barrier unless they are given sufficient energy. After given enough energy (bias), electrons transport over the barrier. This current is equal to

$$J = J_s\left[e^{\frac{eV}{k_BT}} - 1\right] \tag{2.11}$$

where

$$J_s = A^* T^2 e^{-\frac{q\phi_B}{k_BT}} \tag{2.12}$$

is the saturation current. A^* is the Richardson constant, ϕB is the barrier height, kB is the Boltzman constant, q is the elementary charge, T is the temperature.

At higher applied voltage or in case of highly doped semiconductors, current continue to rise and does not saturate. This is because image force lowering which modifies the barrier height or tunneling through the barrier which is called quantum tunneling. The current for such a scenario becomes

$$J_T = J_{TS} e^{-\frac{q\phi_B}{E_\infty}} \tag{2.13}$$

where E represents the characteristic tunneling energy.

2.2.5 Semiconductor Photodetectors

Semiconductor photodetectors are main optoelectronic devices to detect some or all portion of incident light. These photodetectors are semiconductor diodes, however, they are not used for rectification in electronic devices, rather optical detection is important. The main principle is to absorb incident light and convert to current that is also called as photocurrent. Applying the strong electric field under reverse bias helps to improve photogenerated current but thermal generation-recombination current remains the same.

The general principle behind photodetection consist of two steps i) absorption of incident photons which results in electron and hole generation ii) collecting photogenerated electrons and holes at separate poles (contacts) under externally applied electric field.

Photodetector characterizations include analysis of significant figures of merit, which include quantum efficiency, spectral responsivity, detectivity, noise, time response etc. In the content of this thesis, responsivity measurements are performed.

Responsivity, which indicates the quality of converting photons to electrical current, has units of A/W. It is calculated as

$$S = \frac{\eta_{ext} q}{h\nu} = \frac{I_{ph}}{P_{in}} = \eta \frac{\lambda(nm)}{1240(nm)(W/A)} \tag{2.14}$$

where η_{ext} represents the external quantum efficiency, I_{ph} is the photocurrent and P is the optical excitation power. Quantum efficiency is another important parameter and it is closely related to responsivity. It is the number of collected electrons per photon.

2.2.6 MSM Photodetectors

Metal-semiconductor-metal semiconductors consist of two back-to-back Schottky diodes. The contacts of the devices are laterally formed. As a result, the electrodes are kept close to each other to improve collection efficiency of the photogenerated carriers. One Schottky contact is reverse biased to create a depletion layer while the other contact is forward biased to collect the photogenerated carriers. The thickness of the active layer is chosen slightly larger than the absorption length to ensure 100% absorption.

MSM photodiodes are attractive due to their significant advantages such as;

- High-speed and FET compatibility,
- Simple, planar structure is easy to integrate with CMOS technology,
- Low capacitance of devices result in high-speed operation.

The carrier conduction mechanism is thermionic emission under dark environment. This model determines the dark current under low voltages. Since there are two Schottky contacts back to back, we can define the current passing through the device as

$$I_{da} = A_1 A_n{}^{**} T^2 e^{-\frac{q\phi_B}{k_B T}} + A_2 A_p{}^{**} T^2 e^{-\frac{q\phi_B}{k_B T}} \tag{2.15}$$

At higher bias voltages, however, current continue to rise although the thermionic emission current should be saturated. For this case, the phenomenon can be explained as image force lowering which modifies the barrier height or tunneling through the barrier [46].

An important phenomenon seen in MSM photodetectors is persistent photoconductivity. Upon illumination, internal gain may be observed in MSM photodetectors. The internal gain is related to photoconductivity, which is attributed to the long lifetime traps located either within the hetero-interface between contacts and/or the semiconductor surface [46]. After light excitation with energy higher than the band gap energy and under potential difference, the photogenerated holes are trapped at the surface states, and the relaxation times of these holes are longer than the electrons. While electrons are injected out from the semiconductor, identical number of electrons must be injected into the semiconductor to preserve charge neutrality. While holes remain trapped much longer than electrons, the electrons complete multiple cycles that result in additional current through the semiconductor. This mechanism is called photoconductive gain [46]. Photoconductive gain provides over 100% quantum efficiency, which is desired for enhanced detection purposes.

Chapter 3

Experimental Methods

This section describes the film growth, device fabrication, equipment and measurement setups and their working principles which are used for material, electrical and optical characterizations.

3.1 Fabrication Procedure and Equipment

3.1.1 Substrate Selection and Surface Preparation for Growth

To grow semiconductor films on a substrate, substrate selection is substantial. For MSM device purposes, thermally grown Silicon Dioxide on Silicon wafers are used for GaN devices. For ZnO based devices, Silicon substrate is used. Silicon is used as active layer p-type material that forms p-n junction with n-type ZnO film.

Before growth, silicon substrates are cleaned through standard cleaning procedure. First, silicon wafers are immersed into an acid solution (4:1 H_2SO_4:H_2N_2) for 20 minutes to clean any organic contaminants reside on the surface. Then wafers are rinsed with de-ionized (DI) water. Second, wafers are dipped into diluted HF solution (50:1 H_2O:HF) for 1 minute to remove any native oxide on the silicon surface. Then wafers are rinsed with DI water and dried usign Nitrogen flow. After cleaning, samples are directly loaded into deposition chambers.

3.1.2 Silicon Oxide Growth using Plasma Enhanced Chemical Vapor Deposition

To grow an isolation layer on Silicon surface, plasma enhanced chemical vapor deposition (VAKSIS CVD-Handy) is used. A 200nm of SiO_2 layer is deposited. The deposition is done at 1Torr chamber pressure, RF power of 10W at 250°C ambient temperature. N_2O and SiH_4 gases are used with a flow rate of 15sccm and 6sccm respectively. A noble gas He is used for carrier gas with a 700sccm flow rate. The actual chemical reaction is given below:

$$3SiH_4 + 6N_2O \longrightarrow 3SiO_2 + 4NH_3 + 4N_2$$

3.1.3 Film Growth Using Atomic Layer Deposition

In UNAM, a modified version of PA-ALD system is used for III-Nitride film growth. The system includes a stainless steel hollow cathode as a plasma source instead of quartz based inductively coupled RF plasma to reduce serious Oxygen concentration in the films which were previously grown [18]. Hollow cathode plasma system is recently reported for GaN deposition using migration enhanced afterglow [18]. Figure 3.1 shows a photograph of the system that is used for III-Nitride deposition in UNAM.

The deposition temperature is kept below 250°C for all films grown in the study. The precursors used for deposition are shown in Table 3.1. We grow III-Nitride thin films using a plasma source which eliminates the need for thermal energy to increase the reactivity of precursor material (TMGa). In our specific

Figure 3.1: Cambridge NanoTech Fiji F200 PEALD reactor.

Element	Precursor
Gallium (Ga)	Trimethlygallium $Ga(CH)_3$ (TMGa)
Oxygen (O)	Water Vapor (H_2O)
Zinc (Zn)	Dietyhlyzinc $Zn(C_2H_5)_2$ (DEZn)
Nitrogen (N)	N_2:H_2 plasma

Table 3.1: Precursors of GaN and ZnO growth in ALD system.

case, we used hollow cathode plasma source, which helps to reduce the oxygen contamination during the deposition. On the other hand, ZnO films are grown in thermal ALD system. Since precursor for ZnO growth (DEZn) is highly reactive, thermal energy is sufficient to grown high quality films.

3.1.4 Surface Patterning and Photolithography

After film growth, samples are cleaned with acetone, isopropanol and rinsed with deionized water. Then, wafers are dried with nitrogen flow. Next, the wafers are dipped into a diluted HF solution (50:1 H_2O:HF) to remove any native oxide for 1 minute. The wafers are then rinsed and dried with nitrogen. To pattern the surface, wafers are kept at 120°C hot plate for 20 minutes, to eliminate

Figure 3.2: EVG 620 Mask Aligner in UNAM cleanroom facility.

moisture which might result in poor photoresist adhesion. Baked samples are spin coated at 5000 rpm for 40 seconds with Hexamethyldisilazane (HMDS) for an improved conformity and adhesion of the photoresist. Next, a positive photoresist AZ5214 is spin coated at 5000 RPM for 50 seconds. Photoresist layer of 1.4 μm is achieved. The wafers are pre-baked for 50 seconds and exposed to 40mJ UV light with proper masking and alignment using EVG 620 Mask Aligner System. Finally, samples are developed with a 4:1 H_2O:AZ400K developer solution for 30 seconds. Samples are investigated after development to make sure the patterns are transfered without any problems. If patterns are damaged, process is repeated from the first step.

3.1.5 Thermal Evaporator

Thermal evaporation is a kind of physical vapor deposition technique. The metals to be deposited are evaporated and metal atoms deposit on the sample surface. A conductive boat is used to melt the metals. High current is driven through the boat, temperature of the boat rises as current increases. When the evaporation temperature is reached, shutter is opened and deposition starts. The thickness of the coated material is determined tracking the thickness monitor. Deposition parameters for Au, Cr and Al metals are shown in the table below:

Figure 3.3: Vaksis MIDAS Thermal Evaporator PVD/3T.

Metal	Density(g.cm-3)	Acoustic Impedance	Tooling Factor
Gold	19.3	23.18	70
Chromium	7.15	28.95	60
Aluminum	2.7	8.17	50

Table 3.2: Precursors of GaN and ZnO growth in ALD system.

3.1.6 DC Magnetron Sputtering

Sputtering system performs deposition using a plasma source using Argon atoms. For metal deposition DC plasma sources are chosen. Using DC plasma power and continuous Ar flow, the energetic Argon ions hit the target surface and rips atoms off. Removed atoms bond to the substrate surface; as a result, deposition is achieved. The thickness of deposited metals are measured using ellipsometry system. The photo of UNAM's Vaksis MIDAS Magnetron Sputtering system is shown in Figure 3.4. For metallization purposes, Au and Ti are deposited with sputtering system. Performed recipes are given in Table 3.3.

Material	DC Power	Chamber Pressure	Ar Flow	Deposition rate
Gold (Au)	75 W	10 mTorr	50 sccm	25 nm/min
Titanium (Ti)	125 W	10 mTorr	8 sccm	10 nm/min

Table 3.3: Precursors of GaN and ZnO growth in ALD system.

Figure 3.4: DC magnetron sputtering system target deposition parameters.

3.2 Characterization Methods

3.2.1 Photoluminescence Measurement

Photoluminescence (PL) is a material property of light emission due to photon absorption. Given sufficient energy, the electrons are excited to the upper allowable states. Electrons return to their minimum energy position by emitting photons corresponding to the transition energy. This phenomenon is useful for analyzing sub-band gap defect states of materials. Measurements are taken using Cary Eclipse Fluorescence Spectrophotometer to analyze films. The schematic of the measurement system is given in Figure 3.5

Xenon lamp is used to generate the source of the light and the light passes through a monochromator and excitation slit. The sample is placed with an angle slightly higher than 45 degrees in the path of the light. The reflected light should not go into the emission slit since it will cause noise at the detector. The reflection angle can be determined as applying a visible light from the excitation slit and reflected light can be seen with an optical target. After proper alignment, the measurement setup is ready. When optically excited, the sample emits photons in

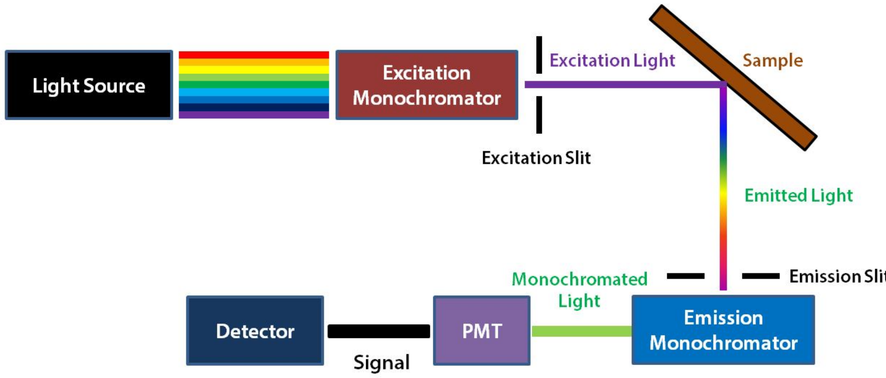

Figure 3.5: Schematic of photoluminescence measurement system.

random directions. The emitted photons incident in emission slit passes through the emission monochromator. The emission monochromator sweeps every wavelength to project the components of emitted light. A small intensity of emitted light is amplified using a photomultiplier tube and pointed into a calibrated optical detector. Optical detector measures intensity of emission with respect to wavelength.

Photoluminescence measurements are taken on GaN and ZnO devices that are coated on silicon dioxide and sapphire respectively.

3.2.2 Spectral Responsivity Measurement

Photodetectors are generally characterized with their measure of responsivity and quantum efficiencies. Responsivity is explained as the photocurrent per incident power and has units Amperes per Watts (A/W). Responsivity measurements are performed using the setup illustrated in Figure 3.6.

A 150 W Xenon lamp is used for light source, which is directly connected to Newport Oriel 1/8m Cornerstone monochromator. The incident monochromatic light modulated using an optical chopper with frequencies much higher than DC to get rid of the flicker noise. Incident light is directed onto photodetectors from

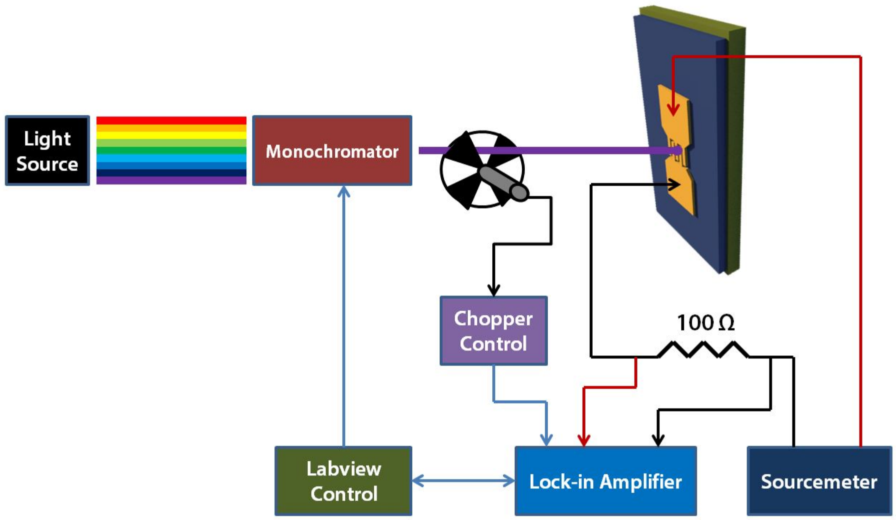

Figure 3.6: Schematic of the responsivity measurement setup.

top. Terminals of the photodetectors are connected to Keithley 2400 sourcemeter using 1 micron tip probes attached to micromanipulators. DC voltages are applied using the sourcemeter.

The photocurrent is recorded using a SRS830 Dual Channel Lock-in Amplifier (Stanford Research Systems). The lock in amplifier is connected in series to the system where total DC current through the circuit is less than 10 μA. If the DC current is higher than 10μA, the photocurrent is extracted measuring the photovoltage of a resistor R and dividing the photovoltage value by the resistor R. The resistor value is chosen such that almost all the applied DC voltage appears across the photodetectors, i.e, the resistor R is much less than the internal resistance of the photodetectors. A 100 ohm resistor is chosen for this purpose.

A Labview user interface is designed so as to automate the measurements over a range of wavelengths. The program communicates with the connected equipment digitally which are lock-in amplifier, monochromator and sourcemeter. User enters lock-in amplification parameters such as sensitivity and time constant, sourcemeter parameters which are initial and final voltage to be applied, the range and step size which the monochromator should scan through. Upon starting the program, monochromator adjusts its slits to wavelength of interest, the

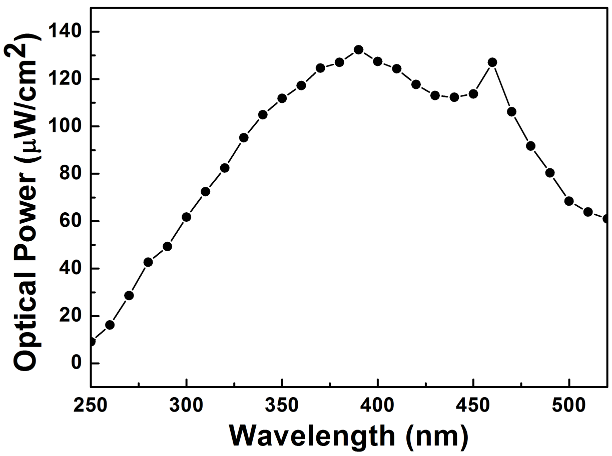

Figure 3.7: Optical Power Spectrum of Responsivity Measurement Setup. The spectrum is measured with a calibrated Silicon photodetector.

lock-in records the current 8 times in a row with an hold time of 0.5 seconds each. 8 data points are recorded and averaged for each incident wavelength. After first 8 data is recorded, the monochromator is set to next wavelength that is simply the initial wavelength plus the stepsize. This loop continues until the final wavelength is reached. The program can also sweep the voltage as well. The recorded photocurrent data at the end is divided by the power recorded using calibrated Silicon photodetector (Newport 918D-UV-ODR3R) connected to an optical powermeter (Newport 1936R). For measurements an optical range between 200 nm to 500 nm is used, optical power is measured after each measurement for every wavelength (Figure 3.7).

3.3 Device Fabrications

3.3.1 MSM Photodetector Fabrications

Silicon wafer with 100-nm-thick SiO_2 layer by PECVD is used for GaN growth. Insulating substrates are used for good electrical isolation. Semi-insulating GaN layer is deposited at 200°C using trimethylgallium ($GaMe_3$) as the Ga precursor and N_2:H_2 (1:1) plasma as nitrogen precursor in an Ultratech/Cambridge Nanotech Fiji F200-LL ALD reactor equipped with a remote hollow-cathode RF-plasma source (Meaglow Ltd.). Following the films deposition, samples are cleaned by acetone, 2-propanol and diluted hydrofluoric acid (HF:H_2O 1:50) solution to remove any native oxide on active layer surface. As a final step, surface is patterned using photolithography with 5μm wide finger-like structure with 5μm spacing in between. Ti (20 nm)/Au (100 nm) contacts are formed using sputtering and lift-off processes. The devices have interdigitated electrodes of 5μm thickness with 5μm spacing between them. Each finger structure has 110μm length as shown in Figure 3.8.

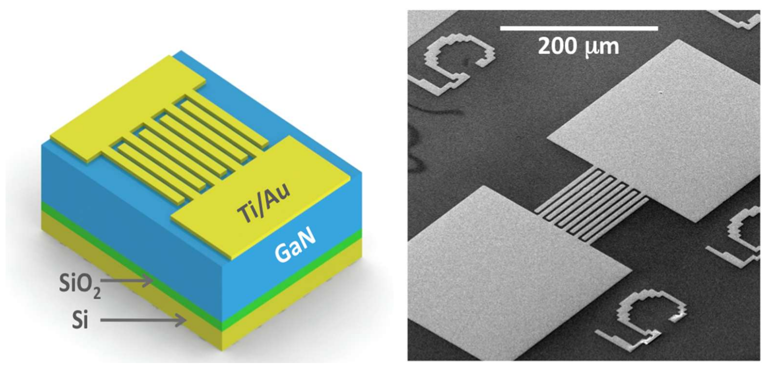

Figure 3.8: a) Schematic illustration of ZnO-Si heterojunction photodiode b) A closer look Scanning Electron Microscope image of the finger-like contacts.

3.3.2 ZnO-Silicon Heterojunction Photodiode Fabrication

As a starting substrate highly doped p-type Si (0.1-0.9 ohm.cm Boron doped) wafers are used. The substrates were dipped into 4:1 H_2SO_4:H_2O_2 solution to clean any organic contaminants. ZnO layers were deposited on Silicon substrates by ALD using a Cambridge Nanotech Savannah 100 system. Various growth temperatures were selected, which are 80°C, 150°C, 200°C and 250°C. Diethlyzinc (DEZn) and water vapor (H_2O) were used as ALD precursors. For each temperature, 300 growth cycles are selected. The growth parameters and deposition rate are given in Table 3.3. For top contact deposition, surface is patterned with photolithography process; Al metal is deposited using a thermal evaporation system. The bottom contact is done with the same method with Al metal. The side of the wafer is covered in order to avoid any electrical shorting. Figure 3.9a shows

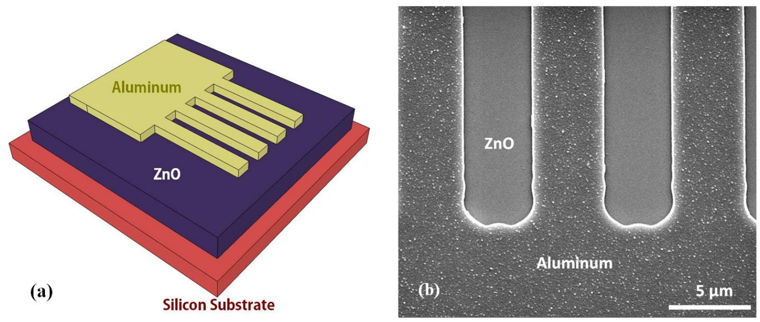

Figure 3.9: a) Schematic illustration of ZnO-Si heterojunction photodiode b) A closer look Scanning Electron Microscope image of the finger-like contacts.

illustration of fabricated device. To make ohmic contact, Al metal is used for top and bottom electrodes. Figure 5.1b shows the scanning electron microscopy image of the photodetector device from top. 5μm wide Al fingers with 5μm spacing is chosen to enable efficient light penetration into the active area.

Temperature (°C)	Pulse Time (s)	Purge Time (s)	Deposition rate (Å/cycle)
80	0.015	60	1.28
150	0.015	60	1.51
200	0.015	10	1.49
250	0.015	5	1.15

Table 3.4: ALD growth parameters of ZnO for different temperatures.

Chapter 4

Hollow Cathode Plasma Assisted Atomic Layer Deposition Based GaN Metal-Semiconductor-Metal Photodetectors

This chapter reports the fabrication, characterization and analysis of GaN based photodetectors. Physical, electrical and optical characteristics are investigated in detail. Part of the work presented in this chapter is published as B. Tekcan, Ç. Özgit-Akgün, S. Bolat, N. Bıyıklı and A. K. Okyay "Metal-semiconductor-metal ultraviolet photodetectors based on gallium nitride grown by atomic layer deposition at low temperatures" in SPIE Optical Engineering Journal, 53 (10), 2014 and as S. Bolat, B. Tekcan, Ç. Özgit-Akgün, N. Biyikli, A. K. Okyay "Electronic and optical device applications of hollow cathode plasma assisted atomic layer deposition based GaN thin films" in Journal of Vacuum Science and Technology A, 33 (1), 2015. Reproduced with permission from The International Society for Optics and Photonics (SPIE) and American Institute of Physics (AIP) publishing.

4.1 Material Analysis

The GIXRD patterns are obtained to examine the crystal quality of GaN films. The peaks indicate a nano-crystalline nature has been achieved. The crystallite size is calculated with Line Profile Analysis (LPA). According to the calculation N_2:H_2 plasma based GaN films has 9.3 nm average size crystals [18]. The field effect charge mobility of the film is extracted using the HCPA-ALD GaN based thin film transistors (TFTs) [47]. The effective charge mobility is 0.025 cm^2/Vsec. This relatively low mobility is attributed to the nanocrystalline nature of the films.

To understand the stoichiometry, XPS elemental analysis is also performed. According to the analysis, films contain 42.19% Ga and 55.18% N after a 60s of in situ Ar etching. The results reveal nitrogen rich film which might create Ga vacancies (V_{Ga}) and/or N interstitials (N_i) and/or N antisites (N_{Ga}). However, the actual nitrogen concentration is slightly less than estimated value due to Auger Ga peaks which are overlapping with N 1s peaks. Moreover, the films contain oxygen less than 1%. However, Ga-O bonds may exist inside the semiconductor which might cause Ga_2O_3 formation that increases the band gap energy.

Photoluminescence measurement is done to take a closer look on the sub-band gap defect levels as well as band-to-band transitions. For this purpose a 20nm thick GaN on Si (111) and c plane sapphire at 200°C are used.

PL spectrum shows multiple peaks in Figure 4.1 under 300nm excitation. There are two peaks located around at 345 and 375nm. They are mixed and appear as a one broader peak. This is believed to be the absorption edge of HCPA-ALD GaN thin films. The peak at 430nm shows a sub-band gap defect assisted green emission. Unlike crystal GaN films, yellow emission is not observable. The green emission is believed to be the origin of persistent photoconductivity. The trap states that cause this green emission peak are located within the forbidden gap and they act to trap one type of charge carrier. The opposite type of charge carrier makes several cycles in the circuit before the trapped charge is released and collected.

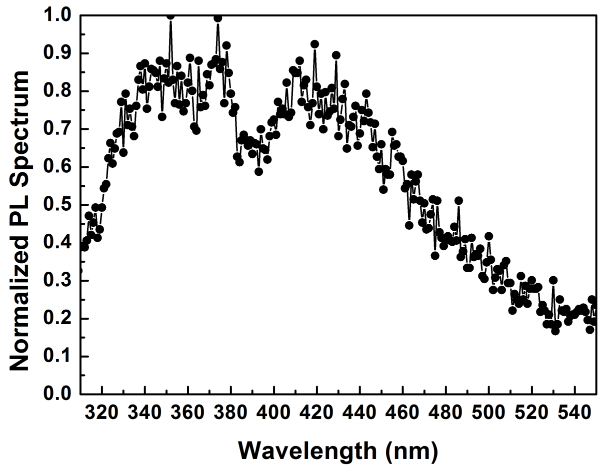

Figure 4.1: Photoluminescence Spectrum of HCPA-ALD GaN excited with 300 nm UV light.

4.2 Electrical Characterizations

Fabricated devices have the metal-semiconductor-metal structure which consists of two back-to-back Schottky diodes. A high work function metal gold (Au) is chosen as contact material to achieve a high Schottky barrier. Titanium (Ti) metal is used for adhesion of Au. An energy band diagram of Ti/Au-GaN-Ti/Au shows the alignment with respect to Fermi energy (Figure 4.2). Neglecting Fermi pinning effect, there is a 0.9eV injection barrier since electron affinity of GaN is 4.1eV and work function of Au metal is 5.1eV.

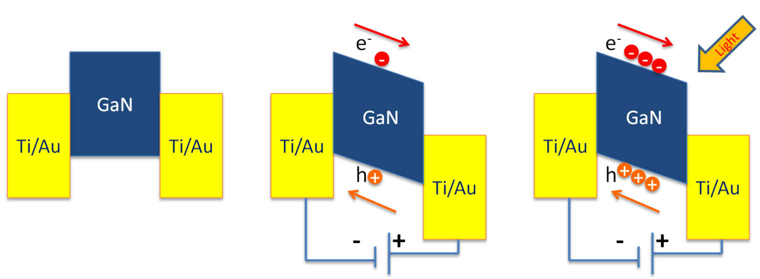

Figure 4.2: Energy band diagram of metal-semiconductor-metal photodetectors a) under thermal equilibrium b) potential difference is applied between contacts c) under light illumination and a potential difference is applied between contacts.

Devices are tested by sweeping the applied bias voltage while simultaneously recording the current through the device. The dark current characteristics are observed from -30V up to 30V as shown in Figure 4.3. Devices exhibit dark current values as low as 14pA under 30V bias. At this range no breakdown characteristics are observed. The current-voltage plot shows a thermionic emission transport mechanism is dominant. The plot follows a linear behavior in logarithmic scale. The linear increase is not as steep as Carrano et. al observed [48], however, one can still claim that a considerable amount of tunneling current is involved.

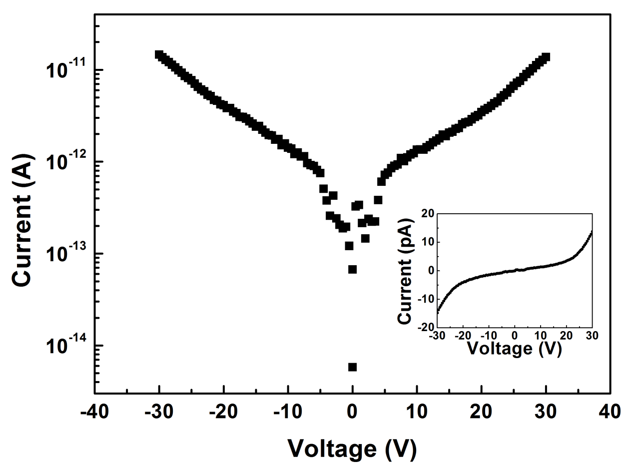

Figure 4.3: Current-Voltage characteristics of the HCPA-ALD grown GaN based MSM photodetectors.

4.3 Optical Characterizations of HCPA-ALD Grown GaN Films

Single crystal MOCVD grown GaN has a band gap of 3.4eV. PA-ALD grown GaN, on the other side, has higher band gap of 3.9eV [45]. As suggested, GaN films have high concentration of oxygen, oxide formation is believed to cause band gap shift towards deeper UV region. The reported value of Ga_2O_3 has band gap of 4.7-5.4eV, which might explain the larger band gap of HCPA-ALD GaN with high amount of oxygen concentration [49, 50]. The shoulder like behavior of transmission for wavelengths lower than 400nm is also attributed to the same reason [45].

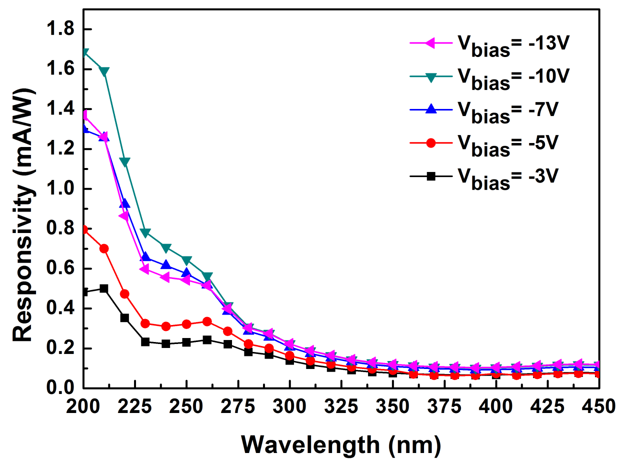

Figure 4.4: Spectral responsivity measurements of HCPA-ALD grown GaN MSM devices under different voltage bias.

Spectral responsivity measurements are in agreement with the optical band gap calculations. The responsivity of as-deposited GaN films (Figure 4.4) with thickness 20nm starts to rise after 315nm which is the extracted band gap energy. Fabricated devices exhibit responsivities 1.687mA/W and 0.101mA/W at 200nm and 390nm, under 10V bias, respectively. Devices show 15x UV/VIS rejection ratio based on responsivity values comparing these two wavelengths. These values are recorded under 10V reverse bias.

Considering the low temperature growth of GaN (below 200°C), the relatively low external quantum efficiency of 1% needs an optimized growth for a better functionality device. The main reason to this quantum efficiency is the low carrier collection efficiency which is attributed to the nano-crystalline structure of the HCPA-ALD grown GaN films. It is believed that many grain boundaries scatter the carriers and reduces the mobility substantially. Moreover, the carrier mobility gets lowered due to scattering effects at the grain boundaries.

Responsivity values increases with voltage bias and saturates after 10V bias. The saturation behavior notifies the complete depletion of 20nm thick GaN film.

The nonzero responsivity for wavelengths higher than band gap, on the other hand, implies a defect-assisted absorption.

To investigate the internal gain mechanism, chopper frequency of responsivity measurement setup is varied while other parameters are kept constant. The responsivity is recorded over the spectrum for different chopper frequencies (Figure 4.6). The results reveal that photoresponse, which must be stable for varied chopper frequencies without any gain mechanism, increases with the chopper frequency. This result shows an internal gain mechanism is present.

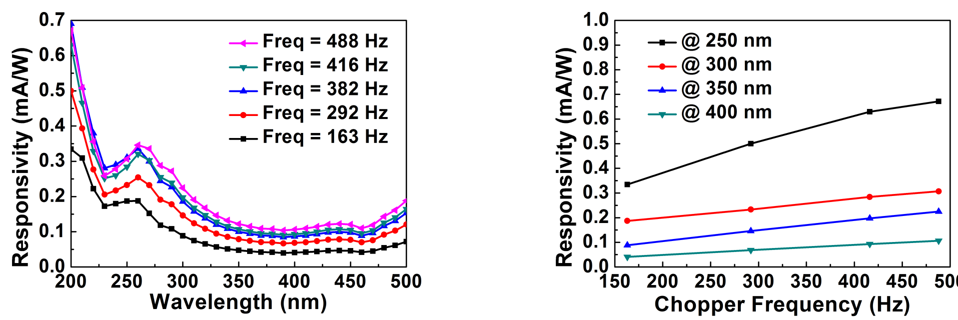

(a) (b)

Figure 4.5: Spectral responsivity of HCPA-ALD grown GaN MSM devices for different chopper frequencies

The origins of the traps are not completely understood. Nevertheless, Nitrogen rich films are presumed to create sub-band gap trap levels. These trap levels are deep and they have acceptor-like nature [51]. Gallium vacancies (V_{Ga}), Nitrogen anti-sites (N_{Ga}) and Nitrogen interstitials (N_i) may create such trap states, resulting in yellow emission, green emission etc [51]. It is believed that these trap levels are responsible for persistent photoconductivity which is observed in the electrical characteristics.

4.4 Post Annealing Study

For post annealing study, as-grown films are kept in rapid thermal annealing (RTA) furnace for 30min at 800°C temperature. Films were annealed either in N_2 gas or N_2:H_2 (forming gas) mixture ambient. Annealing effects in two different ambient are compared with the reference sample. After annealing, the contacts of the devices are fabricated.

We observe a decrease in resistivity of GaN thin films up to 600°C temperature due to hydrogen releasing. However, after 800°C, resistivity drops 40 times. Hydrogen is a well-known element to cause blistering in annealed films after a critical temperature. The films annealed at 800°C showed blistering on the surface. Hydrogen releasing is believed to cause such effect. The SIMS (Secondary Ion Mass Spectroscopy) measurement shows a high concentration of Hydrogen in the as-grown films. Elemental Hydrogen is a good defect eliminator, since it can passivate crystal imperfections and surface dangling bonds. Upon annealing, due to reduced hydrogen concentration, defect based carrier concentration increased. However, the H_2:N_2 annealing resulted in decreased conductivity without blistering. Fabricated devices are electrically tested. Voltage was swept from -30V to

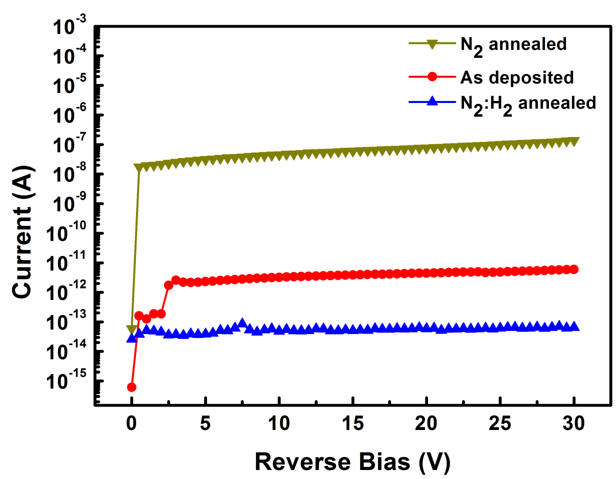

Figure 4.6: Current-voltage characteristics of annealed and as-grown HCPA-ALD grown GaN MSM devices.

30V same as as-grown GaN devices. A current value of 50fA at 20V reverse bias is recorded as shown in Figure 4.7. Devices annealed in N_2:H_2 environment, exhibit two orders of magnitude reduced dark current compared to as grown films. The reduced dark current is attributed to the hydrogen passivation of crystal defects, as well as annealing based crystal quality improvement. The devices based on N_2 annealing, displayed much higher dark currents compared to as-grown GaN devices, on the order of few nA at 20V reverse bias. This behavior might be attributed to hydrogen out-gassing which is explained above.

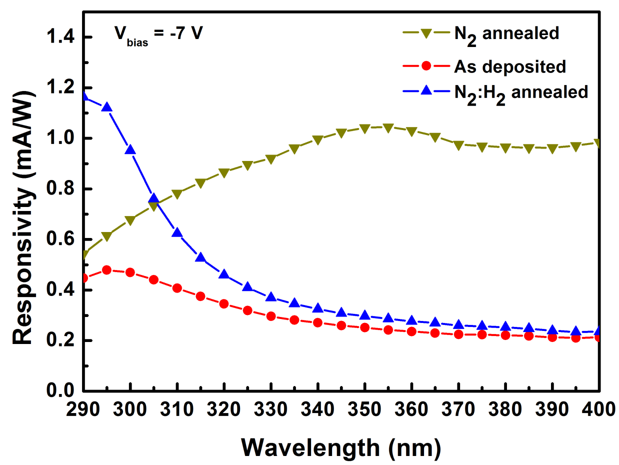

Figure 4.7: Spectral responsivity of annealed and as-grown HCPA-ALD GaN MSM photodetectors.

Responsivity of annealed MSM devices are also investigated. Responsivity values are measured as 0.95mA/W, 0.47mA/W respectively under 7V reverse bias and 300nm wavelength light illumination (Figure 4.7). Annealed GaN films show enhanced responsivity values in the UV regime, possibly due to improved carrier collection efficiency. In the visible side of the spectrum, the picture has changed for both annealed devices as show in Figure 4.7. The responsivity of N_2:H_2 annealed MSM device remained same in the sub-band gap region compared to as-grown films, while N_2 annealed samples showed much higher sub-band gap responsivity. As discussed before, N_2 annealed films seem to become rich in terms of defects and this result in severe sub-band gap transitions. N_2 acts as deep level traps within forbidden gap. As explained in the previous sections, Nitrogen rich

GaN favors negatively charged Ga vacancies, introducing acceptor-like states. Also, N interstitials as well as N anti-sites may be the source of acceptor-like states.

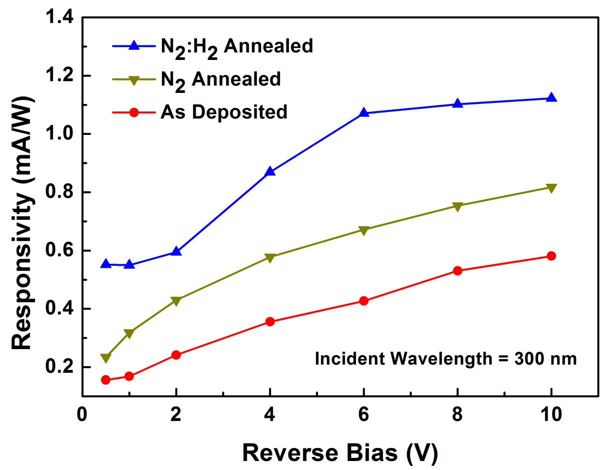

Figure 4.8: Responsivity of HCPA-ALD grown GaN MSM devices with respect to applied reverse bias.

Responsivity values for three different samples seem to increase with voltage bias as shown in Figure 4.8. Curves saturate for high voltages. The saturation behavior is due to complete depletion of the GaN layer below the contacts.

Chapter 5

Atomic Layer Deposition Based ZnO-Si Heterojunction p-n Photodiodes

This chapter presents the electrical and optical characterizations of the ALD grown ZnO-Si heterojunction photodiodes. Part of the work presented in this chapter is published as S. Alkis, B. Tekcan, A. Nayfeh, A. K. Okyay "UV/vis range photodetectors based on thin film ALD grown ZnO/Si heterojunction diodes" in Journal of Optics, 15 (10), 2013. Reproduced with permission from Institute of Physics (IOP) publishing.

The electrical and optical properties can be tuned by ALD deposition temperature. This property is examined in terms of device operation. The junction quality, ON/OFF ratio of the diode was studied. Responsivities of the photodetectors are measured to assess the photon to current conversion efficiency.

5.1 Material Characteristics

The ALD grown ZnO film resistivities measured (Figure 5.1) with a Van Der Pauw structure are in agreement with the previously reported values.

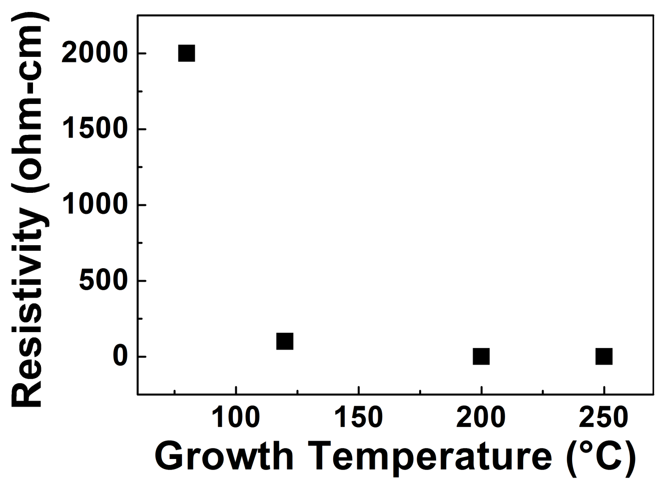

Figure 5.1: Resistivity values of ZnO films grown at different temperatures.

The mobility values are extracted from linear region current of ALD ZnO based TFTs [52]. For 80°C based ZnO films, the field effect electron mobility is 3.96cm^2/V-sec. The bulk mobility is expected to be higher than field effect mobility due to surface states. However, the extracted value is larger than amorphous silicon electron mobility, which gives a good insight to assess the crystal quality.

To investigate sub-band gap transitions, a PL spectrum is measured under 250nm (Figure 5.2a) and 390nm (Figure 5.2b) wavelength light excitations. The PL spectrum shows three major peaks under 250nm illumination, located at 376nm, 426nm and 500nm. The peak at 376nm shows the band-to-band emission of ZnO films, corresponding to energy of 3.3eV. PL signal at 426nm is due to a transition from conduction band to Zinc vacancy state and/or from Zinc interstitial to Zinc vacancy state [36]. The peak at 500nm is second harmonic effect of incident wavelength reflected from the sample surface. PL peaks measured under 390nm excitation agree well with the 250nm excitation measurements. The peak

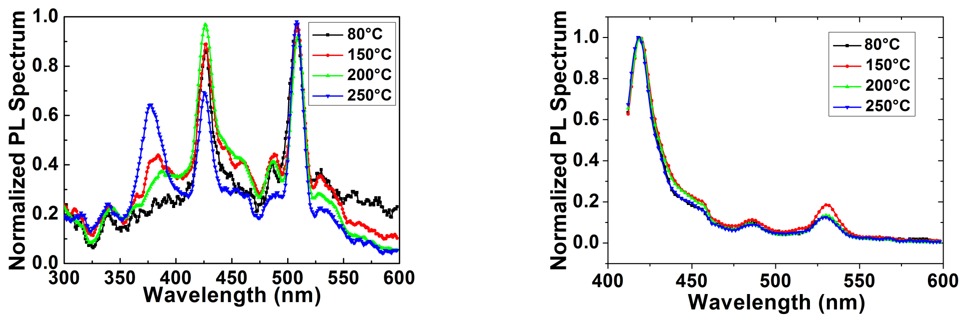

(a) (b)

Figure 5.2: Photoluminescence spectra of ZnO films a) excitation wavelength is 250nm b) excitation wavelength is 390nm.

seen at 418nm shows the same defect state transition since 390nm excitation is not sufficient to activate band-to-band transmission (excitation). We do not see the peak around 376nm. The peak at 500nm disappeared since the second harmonic of the light source is at 780nm.

5.2 Current-Voltage Characteristics

Unintentionally doped ZnO layers are estimated to have electron rich n-type characteristics due to oxygen vacancies and Zn interstitials although there is still debate about the origin of dominant carrier type. Electrical characterization is performed to evaluate the diode quality of n-type ZnO with p-type Si substrate. Current-voltage characteristics of various ZnO deposition temperature based devices are examined as plotted in Figure 5.3. 80°C grown ZnO-Si heterojunction showed highest rectification ratio among others. These devices showed decent electrical characteristics with 10^3 ON to OFF ratio. Carrier concentration of ZnO becomes comparable to Si substrate as increasing the deposition temperature, shortening the depletion region at the Si side. So the ON to OFF ratio decreased significantly.

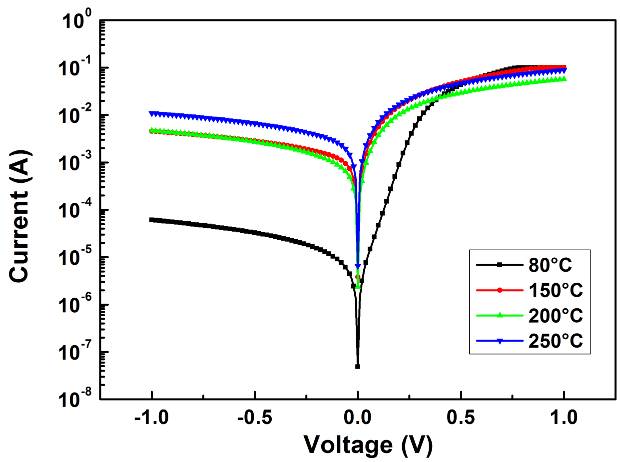

Figure 5.3: Current-Voltage characteristics of ZnO-Silicon heterojunction photodiodes. The graph contains different temperature grown ZnO layers.

5.3 Responsivity Analysis

Responsivity values were calculated measuring the photocurrent and scaling it with the optical power of the incident light. Responsivity is calculated as a function of voltage bias under λ = 350nm (UV) and λ = 475nm (VIS). Please note that power at UV is 5.84x10^{-5} W and 8.88x10^{-5} W for VIS.

Under UV illumination, responsivity shows a steep increase <0.2V reverse bias, saturates for voltages higher than 0.2V, as shown in Figure 5.4a. This increase is attributed to efficient carrier collection efficiency with applied reverse bias, while saturation of carrier drift velocity due to scattering inside the crystal explains constant responsivity for higher voltages. The measured responsivity values are 37mA/W (80°C), 35mA/W (250°C) and 30mA/W (150°C, 200°C) at 0.5V. Highest responsivity of 80°C device can be related to the near stoichiometry of Zn:O atoms, at the particular temperature [22]. At higher temperature, however, the stoichiometry decreases since oxygen concentration decreases.

Figure 5.4b shows illumination under VIS light (λ=475nm). The voltage bias dependency is similar to UV illuminated case, as saturation occurs after 0.2V.

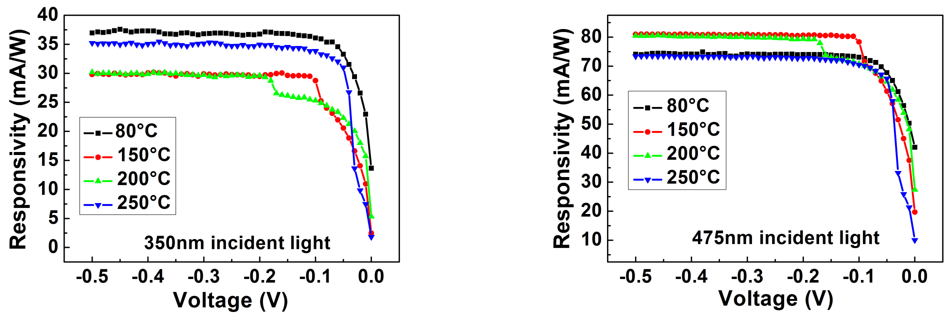

(a) (b)

Figure 5.4: Responsivity spectra of ZnO-Silicon heterojunction photodiodes with respect to the applied voltage between positive and negative contacts a) under 350nm b) under 475nm incident light. Negative voltage corresponds to reverse bias.

The responsivity values are 37mA/W (80°C), 35mA/W (250°C) and 30mA/W (150°C, 200°C) at 0.5V. While 80°C has the highest UV responsivity, 150°C has the highest responsivity in the visible region.

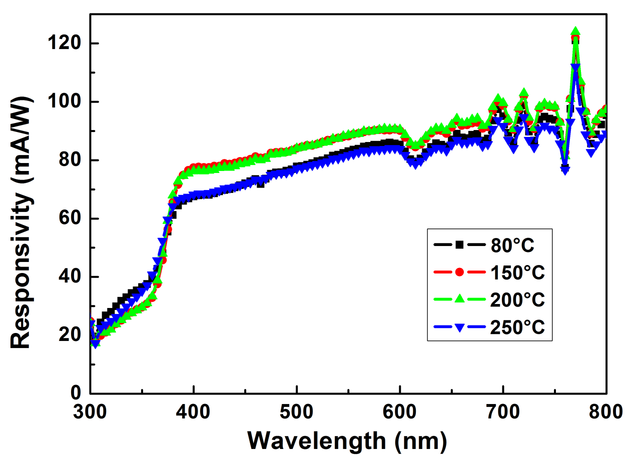

Figure 5.5: Responsivity spectrum of ZnO-Silicon heterojunction photodiodes with respect to illumination wavelength.

Finally, responsivity as a function of illumination wavelength is observed in Figure 5.5. A wide range from 300nm up to 800nm is investigated under 0.5V bias. Maximum responsivity values of 85mA/W (80°C), 90mA/W (150°C, 200°C) and 84mA/W (250°C) are recorded at 585nm. Figure 5.5 demonstrates an efficient operation of photodetection from UV to NIR covering all visible range.

Chapter 6

Conclusion

GaN and ZnO, both having wurtzite crystal structure have direct band gap around 3.3-3.4eV. Due to electrical and optical properties of these two materials, they are under intensive study. Traditional growth techniques offer high crystal quality; however, the need for high temperature process hinders the growth of GaN and ZnO on temperature sensitive applications such as flexible electronics and CMOS planar integration. At higher temperature such substrates face with serious degradation, as a result, it is impossible to use these traditional growth techniques for particular applications.

Among other techniques, ALD is a useful method in terms of step coverage, very sensitive thickness control and low temperature growth. Taking advantage of unique properties of ALD, our aim was to investigate the feasibility of ALD based photodetectors based on ALD grown semiconductors.

In the first part of the thesis, HCPA-ALD grown GaN films were used to fabricate metal-semiconductor-metal photodetectors. Material characteristics of the as grown films were examined. GIXRD peaks revealed a polycrystalline nature GaN with a grain size of 9.3nm is achieved. Nitrogen-rich GaN layers were verified by XPS analysis. Finally photoluminescence spectrum was investigated, green emission peak which corresponds to a state within the forbidden gap is observed.

Photodetectors were fabricated by forming Ti/Au Schottky contacts by lift-off process. Devices were electrically and optically characterized. Devices exhibit very low dark current of 14pA under 20V bias. This is due to both high Schottky barrier height and low resistivity of HCPA-ALD GaN films. Nano-crystalline nature of GaN with 9.3nm grain size affected responsivity significantly due to grain boundary scattering as well as possible formation of Gallium vacancies, N-interstitials or N-antisites. A UV/VIS rejection ratio was calculated as 15 comparing the responsivity values at 200nm and 390nm wavelengths respectively. The responsivity value at 200nm and 390nm are measured as 1.687mA/W and 0.101mA/W, respectively. Moreover, photoconductive gain mechanism was investigated by varying optical chopper frequency of the responsivity measurement system. Increase in responsivity with chopper frequency was observed which is attributed to different carrier lifetime of electrons and holes. It is believed that the different lifetime of the carriers contribute to the persistent photoconductivity.

We have demonstrated, for the first time, a very low temperature grown GaN based on HCPA-ALD technique and analyzed metal-semiconductor-metal photodetectors fabricated from those GaN layers. Initial results are promising, however, a further improvement in the film quality is needed for high performance devices. It is estimated that functional devices based on HCPA-ALD technique offers an alternative to electronic devices based on conventional growth methods.

In the second part of the thesis, ALD grown ZnO is used to form a heterojunction photodiode with Silicon. ZnO is unintentionally grown as n-type and ALD growth temperature determines the carrier concentration of ZnO. As a result, there is an opportunity to tune electrical characteristics of ZnO layers. Effect of growth temperature of ZnO layers on device performance is observed.

To investigate defect states, photoluminescence measurements were performed. Two distinct peaks around 376nm and 418nm are observed. The PL peaks were sharp that was an indication of high quality films. The resistivity of films were measured using Van Der Pauw structures. We observed that increase in deposition temperature increases the carrier concentration significantly especially beyond 200°C.

Electrical current voltage characteristics of the corresponding devices were investigated. While 80°C grown ZnO based device had an rectification ratio of 10^3, 150°C, 200°C and 250°C grown ZnO-Si heterostructure photodiodes exhibited a low rectification ratio. Responsivity values of 37mA/W (80°C), 35mA/W (250°C) and 30mA/W (150°C, 200°C) at 0.5V were recorded under an illumination of 300nm wavelength. On the visible side, however, 85mA/W (80°C), 90mA/W (150°C, 200°C) and 84mA/W (250°C) are recorded at 585nm. The wide responsivity with decent values show promise in various solar cell and photodetector applications based on ZnO.

Both studies showed the realization of ALD based optoelectronic devices with decent quality. As a future work, these devices could be formed on temperature sensitive substrates such as flexible films or CMOS integrated circuits. Since both ZnO and GaN are promising materials, ALD integration of these materials can pave the way to a new class of electronic and photonics device applications. Moreover, film quality always puts a challenge on device quality. Grown films mentioned in the thesis can be used for commercial purposes if the film quality is improved.

Bibliography

[1] M. Ritala, J. Niinisto, S. Krumdieck, P. Chalker, H. Aspinall, M. E. Pemble, W. L. Gladfelter, B. Leese, R. A. Fischer, H. Parala, R. Kanjolia, R. D. Dupuis, S. E. Alexandrov, S. J. C. Irvine, R. Palgrave, and I. P. Parkin, *Chemical Vapour Deposition*. The Royal Society of Chemistry, 2009.

[2] S. M. George, "Atomic layer deposition: an overview," *Chemical reviews*, vol. 110, no. 1, pp. 111–131, 2009.

[3] S. Bloom, G. Harbeke, E. Meier, and I. Ortenburger, "Band structure and reflectivity of gan," *physica status solidi (b)*, vol. 66, no. 1, pp. 161–168, 1974.

[4] J. Carrano, T. Li, P. Grudowski, C. Eiting, R. Dupuis, and J. Campbell, "High quantum efficiency metal-semiconductor-metal ultraviolet photodetectors fabricated on single-crystal gan epitaxial layers," *Electronics Letters*, vol. 33, no. 23, pp. 1980–1981, 1997.

[5] F. Xie, H. Lu, X. Xiu, D. Chen, P. Han, R. Zhang, and Y. Zheng, "Low dark current and internal gain mechanism of gan msm photodetectors fabricated on bulk gan substrate," *Solid-State Electronics*, vol. 57, no. 1, pp. 39–42, 2011.

[6] J. Li, Y. Xu, T. Hsiang, and W. Donaldson, "Picosecond response of gallium-nitride metal–semiconductor–metal photodetectors," *Applied physics letters*, vol. 84, no. 12, pp. 2091–2093, 2004.

[7] S.-J. Chang, M. Lee, J.-K. Sheu, W. Lai, Y.-K. Su, C. Chang, C. Kao, G.-C. Chi, and J. Tsai, "Gan metal-semiconductor-metal photodetectors with low-temperature-gan cap layers and ito metal contacts," *Electron Device Letters, IEEE*, vol. 24, no. 4, pp. 212–214, 2003.

[8] N. Biyikli, T. Kartaloglu, O. Aytur, I. Kimukin, and E. Ozbay, "High-speed visible-blind gan-based indium–tin–oxide schottky photodiodes," *Applied Physics Letters*, vol. 79, no. 17, pp. 2838–2840, 2001.

[9] S. Butun, N. A. Cinel, and E. Ozbay, "Lspr enhanced msm uv photodetectors," *Nanotechnology*, vol. 23, no. 44, p. 444010, 2012.

[10] H. Wu, Y. Sun, D. Lin, R. Zhang, C. Zhang, and W. Pan, "Gan nanofibers based on electrospinning: facile synthesis, controlled assembly, precise doping, and application as high performance uv photodetector," *Advanced Materials*, vol. 21, no. 2, pp. 227–231, 2009.

[11] W.-Y. Weng, T.-J. Hsueh, S.-J. Chang, S.-B. Wang, H.-T. Hsueh, and G.-J. Huang, "A high-responsivity gan nanowire uv photodetector," *Selected Topics in Quantum Electronics, IEEE Journal of*, vol. 17, no. 4, pp. 996–1001, 2011.

[12] R. W. Chuang, S. Chang, S.-J. Chang, Y. Chiou, C. Lu, T. Lin, Y. Lin, C. Kuo, and H.-M. Chang, "Gallium nitride metal-semiconductor-metal photodetectors prepared on silicon substrates," *Journal of Applied Physics*, vol. 102, no. 7, p. 073110, 2007.

[13] A. Osinsky, S. Gangopadhyay, J. Yang, R. Gaska, D. Kuksenkov, H. Temkin, I. Shmagin, Y.-C. Chang, J. Muth, and R. Kolbas, "Visible-blind gan schottky barrier detectors grown on si (111)," *Applied physics letters*, vol. 72, no. 5, pp. 551–553, 1998.

[14] M. Mikulics, M. Marso, P. Javorka, P. Kordos, H. Luth, M. Kocan, A. Rizzi, S. Wu, and R. Sobolewski, "Ultrafast metal-semiconductor-metal photodetectors on low-temperature-grown gan," *Applied physics letters*, vol. 86, no. 21, pp. 211110–211110, 2005.

[15] S. Wang, T. Li, J. Reifsnider, B. Yang, C. Collins, A. Holmes, and J. Campbell, "Schottky metal-semiconductor-metal photodetectors on gan films grown on sapphire by molecular beam epitaxy," *IEEE journal of quantum electronics*, vol. 36, no. 11, pp. 1262–1266, 2000.

[16] E. Knox-Davies, J. Shannon, and S. Silva, "The properties and deposition process of gan films grown by reactive sputtering at low temperatures," *Journal of applied physics*, vol. 99, no. 7, 2006.

[17] T. Huang, E. Tuncel, J. Yeo, and J. Harris, "Growth of epitaxial gan films using zno buffer layer by pulsed laser deposition," in *MRS Proceedings*, vol. 421, p. 389, Cambridge Univ Press, 1996.

[18] C. Ozgit-Akgun, E. Goldenberg, A. K. Okyay, and N. Biyikli, "Hollow cathode plasma-assisted atomic layer deposition of crystalline aln, gan and al x ga 1- x n thin films at low temperatures," *Journal of Materials Chemistry C*, vol. 2, no. 12, pp. 2123–2136, 2014.

[19] H. Kim, J. Kim, Y. Kim, K. Chae, C. Whang, J. Song, and S. Im, "Photoresponse of si detector based on n-zno/p-si and n-zno/n-si structures," *Optical materials*, vol. 17, no. 1, pp. 141–144, 2001.

[20] S. Faÿ, L. Feitknecht, R. Schlüchter, U. Kroll, E. Vallat-Sauvain, and A. Shah, "Rough zno layers by lp-cvd process and their effect in improving performances of amorphous and microcrystalline silicon solar cells," *Solar Energy Materials and Solar Cells*, vol. 90, no. 18, pp. 2960–2967, 2006.

[21] A. Janotti and C. G. Van de Walle, "Fundamentals of zinc oxide as a semiconductor," *Reports on Progress in Physics*, vol. 72, no. 12, p. 126501, 2009.

[22] C. Park, I. Jeong, J. Kim, and S. Im, "Spectral responsivity and quantum efficiency of n-zno/p-si photodiode fully isolated by ion-beam treatment," *Applied physics letters*, vol. 82, no. 22, pp. 3973–3975, 2003.

[23] J. Lee, Y. Choi, W. Choi, H. Yeom, Y. Yoon, J. Kim, and S. Im, "Characterization of films and interfaces in n-zno/p-si photodiodes," *Thin Solid Films*, vol. 420, pp. 112–116, 2002.

[24] F. Chaabouni, M. Abaab, and B. Rezig, “Characterization of n-zno/p-si films grown by magnetron sputtering,” *Superlattices and Microstructures*, vol. 39, no. 1, pp. 171–178, 2006.

[25] R. Groenen, J. Löffler, P. Sommeling, J. Linden, E. Hamers, R. Schropp, and M. Van de Sanden, “Surface textured zno films for thin film solar cell applications by expanding thermal plasma cvd,” *Thin Solid Films*, vol. 392, no. 2, pp. 226–230, 2001.

[26] P. Peumans, A. Yakimov, and S. R. Forrest, “Small molecular weight organic thin-film photodetectors and solar cells,” *Journal of Applied Physics*, vol. 93, no. 7, pp. 3693–3723, 2003.

[27] S. Alkis, T. Öztaş, L. Aygün, F. Bozkurt, A. Okyay, and B. Ortaç, “Thin film mos 2 nanocrystal based ultraviolet photodetector,” *Optics express*, vol. 20, no. 19, pp. 21815–21820, 2012.

[28] S.-W. Seo, S.-Y. Cho, S. Huang, J. J. Shin, N. M. Jokerst, A. S. Brown, M. Brooke, *et al.*, “High-speed large-area inverted ingaas thin-film metal-semiconductor-metal photodetectors,” *Selected Topics in Quantum Electronics, IEEE Journal of*, vol. 10, no. 4, pp. 686–693, 2004.

[29] I.-S. Jeong, J. H. Kim, and S. Im, “Ultraviolet-enhanced photodiode employing n-zno/p-si structure,” *Applied physics letters*, vol. 83, no. 14, pp. 2946–2948, 2003.

[30] L. Shen, Z. Ma, C. Shen, F. Li, B. He, and F. Xu, “Studies on fabrication and characterization of a zno/p-si-based solar cell,” *Superlattices and Microstructures*, vol. 48, no. 4, pp. 426–433, 2010.

[31] J. Ye, S. Gu, S. Zhu, W. Liu, S. Liu, R. Zhang, Y. Shi, and Y. Zheng, “Electroluminescent and transport mechanisms of n-zno/p-si heterojunctions,” *Applied Physics Letters*, vol. 88, no. 18, p. 2112, 2006.

[32] S. Tan, X. Sun, J. Zhao, S. Iwan, Z. Cen, T. Chen, J. Ye, G. Lo, D. Kwong, and K. Teo, “Ultraviolet and visible electroluminescence from n-zno/siox/(n, p)-si heterostructured light-emitting diodes,” *Applied Physics Letters*, vol. 93, no. 1, pp. 13506–13900, 2008.

[33] A. Ibrahim and A. Ashour, "Zno/si solar cell fabricated by spray pyrolysis technique," *Journal of Materials Science: Materials in Electronics*, vol. 17, no. 10, pp. 835–839, 2006.

[34] E. Yousfi, B. Weinberger, F. Donsanti, P. Cowache, and D. Lincot, "Atomic layer deposition of zinc oxide and indium sulfide layers for cu (in, ga) se 2 thin-film solar cells," *Thin Solid Films*, vol. 387, no. 1, pp. 29–32, 2001.

[35] N. Huby, G. Tallarida, M. Kutrzeba, S. Ferrari, E. Guziewicz, M. Godlewski, *et al.*, "New selector based on zinc oxide grown by low temperature atomic layer deposition for vertically stacked non-volatile memory devices," *Microelectronic Engineering*, vol. 85, no. 12, pp. 2442–2444, 2008.

[36] E. Guziewicz, I. Kowalik, M. Godlewski, K. Kopalko, V. Osinniy, A. Wójcik, S. Yatsunenko, E. Łusakowska, W. Paszkowicz, and M. Guziewicz, "Extremely low temperature growth of zno by atomic layer deposition," *Journal of Applied Physics*, vol. 103, no. 3, p. 033515, 2008.

[37] A. B. Martinson, J. W. Elam, J. T. Hupp, and M. J. Pellin, "Zno nanotube based dye-sensitized solar cells," *Nano letters*, vol. 7, no. 8, pp. 2183–2187, 2007.

[38] G. Luka, P. Stakhira, V. Cherpak, D. Volynyuk, Z. Hotra, M. Godlewski, E. Guziewicz, B. Witkowski, W. Paszkowicz, and A. Kostruba, "The properties of tris (8-hydroxyquinoline) aluminum organic light emitting diode with undoped zinc oxide anode layer," *Journal of Applied Physics*, vol. 108, no. 6, p. 064518, 2010.

[39] T. Krajewski, G. Łuka, B. Witkowski, B. Kowalski, K. Kopalko, J. Domagala, M. Guziewicz, M. Godlewski, E. Guziewicz, *et al.*, "Monocrystalline zinc oxide films grown by atomic layer deposition," *Thin Solid Films*, vol. 518, no. 16, pp. 4556–4559, 2010.

[40] F. B. Oruç, F. Cimen, A. Rizk, M. Ghaffari, A. Nayfeh, and A. K. Okyay, "Thin-film zno charge-trapping memory cell grown in a single ald step," *Electron Device Letters, IEEE*, vol. 33, no. 12, pp. 1714–1716, 2012.

[41] J. Ren, “Initial growth mechanism of atomic layer deposition of zno on the hydroxylated si (100)-2× 1: A density functional theory study,” *Applied Surface Science*, vol. 255, no. 11, pp. 5742–5745, 2009.

[42] E. Guziewicz, M. Godlewski, L. Wachnicki, T. Krajewski, G. Luka, S. Gieraltowska, R. Jakiela, A. Stonert, W. Lisowski, M. Krawczyk, *et al.*, “Ald grown zinc oxide with controllable electrical properties,” *Semiconductor Science and Technology*, vol. 27, no. 7, p. 074011, 2012.

[43] T. Suntola and J. Antson, “Method for producing compound thin films,” Nov. 15 1977. US Patent 4,058,430.

[44] M. Leskelä and M. Ritala, “Atomic layer deposition chemistry: recent developments and future challenges,” *Angewandte Chemie International Edition*, vol. 42, no. 45, pp. 5548–5554, 2003.

[45] E. Goldenberg, C. Ozgit-Akgun, N. Biyikli, and A. K. Okyay, “Optical characteristics of nanocrystalline alxga1-xn thin films deposited by hollow cathode plasma-assisted atomic layer deposition,” *Journal of Vacuum Science & Technology A*, vol. 32, no. 3, p. 031508, 2014.

[46] S. M. Sze and K. K. Ng, *Physics of semiconductor devices.* John Wiley & Sons, 2006.

[47] S. Bolat, C. Ozgit-Akgun, B. Tekcan, N. Biyikli, and A. Okyay, “Low temperature thin film transistors with hollow cathode plasma-assisted atomic layer deposition based gan channels,” *Applied Physics Letters*, vol. 104, no. 24, p. 243505, 2014.

[48] J. Carrano, T. Li, D. Brown, P. Grudowski, C. Eiting, R. Dupuis, and J. Campbell, “Very high-speed metal-semiconductor-metal ultraviolet photodetectors fabricated on gan,” *Applied physics letters*, vol. 73, no. 17, pp. 2405–2407, 1998.

[49] D.-w. Choi, K.-B. Chung, and J.-S. Park, “Low temperature ga 2 o 3 atomic layer deposition using gallium tri-isopropoxide and water,” *Thin Solid Films*, vol. 546, pp. 31–34, 2013.

[50] K. Sasaki, M. Higashiwaki, A. Kuramata, T. Masui, and S. Yamakoshi, "Mbe grown ga 2 o 3 and its power device applications," *Journal of Crystal Growth*, vol. 378, pp. 591–595, 2013.

[51] M. A. Reshchikov and H. Morkoc, "Luminescence properties of defects in gan," *Journal of applied physics*, vol. 97, no. 6, p. 061301, 2005.

[52] L. E. Aygun, F. B. Oruc, F. B. Atar, and A. K. Okyay, "Dynamic control of photoresponse in zno-based thin-film transistors in the visible spectrum," *Photonics Journal, IEEE*, vol. 5, no. 2, pp. 2200707–2200707, 2013.